Dissertation
submitted to the
Combined Faculties for the Natural Sciences and for Mathematics
of the Ruperto-Carola University of Heidelberg, Germany
for the degree of
Doctor of Natural Sciences

presented by

Atif Shahbaz
born in Lahore, Pakistan

Oral examination: January 28th, 2009

Muonic Atoms

in

Super-Intense Laser Fields

Referees: **Prof. Dr. Christoph H. Keitel**

Prof. Dr. Thomas Stöhlker

Zusammenfassung

Es werden Kerneffekte in wasserstoff-ähnlichen myonischen Atomen, die intensiver Laserstrahlung hoher Frequenz ausgesetzt sind, untersucht. Dabei werden Systeme mit niedriger Kernladungszahl betrachtet, die eine nichtrelativistische Beschreibung erlauben. Durch Vergleich der von verschiedenen Isotopen ausgesandten hochharmonischen Strahlung werden charakteristische Signaturen durch die Kernmasse, -größe und -form demonstriert. Maximale Photonenenergien im MeV-Bereich sind erreichbar und weisen einen Weg zur Erzeugung ultra-kurzer, kohärenter γ-Pulse. Darüber hinaus kann der Atomkern durch die laser-getriebene periodische Bewegung des Myons angeregt werden. Der Übergang in ein höheres Kernniveau wird durch das zeitabhängige Coulomb-Feld der oszillierenden Ladungsdichte des gebundenen Myons hervorgerufen. Im Rahmen eines vollständig quantenmechanischen Ansatzes wird ein geschlossener analytischer Ausdruck für elektrische Multipolübergänge hergeleitet und auf verschiedene Isotope angewandt. Die Anregungswahrscheinlichkeiten sind im Allgemeinen sehr klein. Wir vergleichen den Prozess mit anderen Kernanregungsmechanismen, die auf einer Kopplung mit der atomaren Hülle beruhen, und diskutieren die Aussichten für seine experimentelle Beobachtung.

Abstract

Nuclear effects in hydrogenlike muonic atoms exposed to intense high-frequency laser fields have been studied. Systems of low nuclear charge number are considered where a nonrelativistic description applies. By comparing the radiative response for different isotopes we demonstrate characteristic signatures of the finite nuclear mass, size and shape in the high-harmonic spectra. Cutoff energies in the MeV domain can be achieved, offering prospects for the generation of ultrashort coherent γ-ray pulses. Also, the nucleus can be excited while the laser-driven muon moves periodically across it. The nuclear transition is caused by the time-dependent Coulomb field of the oscillating charge density of the bound muon. A closed-form analytical expression for electric multipole transitions is derived within a fully quantum mechanical approach and applied to various isotopes. The excitation probabilities are in general very small. We compare the process with other nuclear excitation mechanisms through coupling with atomic shells and discuss the prospects to observe it in experiment.

In connection with the work on this thesis, the following articles were published in refereed journals:

- A. Shahbaz, C. Müller, A. Staudt, T. J. Bürvenich, and C. H. Keitel: *Nuclear signatures in high-harmonic generation from laser-driven muonic atoms*
  Phys. Rev. Lett. **98**, 263901 (2007).

  [selected for volume 6, issue 7 of the "Virtual Journal of Ultrafast Science" (`http://www.vjultrafast.org`), publishers: APS, AIP]

- C. Müller, A. D. Piazza, A. Shahbaz, T. J. Bürvenich, J. Evers, K. Z. Hatsagortsyan and C. H. Keitel: *High-energy, nuclear and QED processes in strong laser fields*
  Laser Phys. 18, 175 (2008).

- C. Müller, A. Shahbaz, T. J. Bürvenich, K. Z. Hatsagortsyan and C. H. Keitel: *Exotic Atoms in Superintense Laser Fields*
  (accepted in Eur. Phys. J. Spec. Top.)

Articles to be submitted:

- A. Shahbaz, C. Müller, T. J. Bürvenich, and C. H. Keitel: *Isotope effects in the harmonic response from hydrogenlike muonic atoms in strong laser fields*
  to be submitted

- A. Shahbaz, C. Müller, T. J. Bürvenich, and C. H. Keitel: *Laser-induced nuclear excitation in muonic atoms*
  to be submitted

Unrefereed publications:

- C. Müller, A. Pálffy, A. Ipp, A. Shahbaz, A. Di Piazza, T. J. Bürvenich, J. Evers, and C. H. Keitel: *Coupling of nuclear matter to intense photon fields*
  GSI Report 2008-05, April 2008, 26-32.

Contents

1 Introduction **9**

2 Laser-Atom Interaction and High Harmonic Generation **15**

2.1 Introduction 15

2.2 Multiphoton Ionization 15

2.3 Keldysh Theory 17

2.4 High harmonic generation (HHG) 21

2.4.1 HHG spectrum 21

2.4.2 Three-step model 22

2.4.3 Applications of HHG 23

2.5 Strong-field phenomena at very high intensities 24

3 Muonic Atoms **27**

3.1 Introduction 27

3.2 Formation of a muonic atom 27

3.3 Traditional applications of muonic atoms for nuclear spectroscopy 28

3.4 Muonic atoms in laser beams 30

3.4.1 Separation of Relative and Center of Mass Motion and Scaling of Muonic Atoms 30

3.4.2 Scaling laws 32

4 Muonic Atoms and Nuclear Spectroscopy via HHG **33**

4.1 Introduction 33

4.2 Model Potentials 33

4.3 HHG of muonic hydrogen isotopes 36

4.3.1 Nuclear mass effect 37

4.3.2 Nuclear size effect 38

4.3.3 Justification of Dipole approximation 39
4.4 HHG for muonic atoms with Z>1 40
4.4.1 Nuclear mass effect 40
4.4.2 Nuclear size effect 43
4.4.3 Comparison with electronic systems 50
4.5 Effects of the nuclear shape 51
4.6 Conclusion 51

5 Nuclear Excitation in Muonic Atoms with Ultraintense Laser Fields 53
5.1 Introduction 53
5.2 Oscillation of the muon via Monte Carlo simulation 54
5.3 Nuclear Excitation by coherent muon motion 54
5.4 Results 61
5.5 Comparison with related processes 64

6 Conclusion and outlook 65

A Cut-off law of HHG 67

B Separation without dipole approximation 69

C Crank Nicholson Scheme 71

D Dipole, quadrupole and octupole transitions 77

Bibliography 79

Chapter 1

Introduction

It has always been a part of human curiosity to aspire more knowledge about nature. To explore the fundamental laws of nature, one has to go to the microworld and that is only possible via technology. With the advent of Quantum Mechanics, we are already into the world of the objects which we are unable to see on our own. With the discoveries of atom and atomic nucleus, we are in a totally different world which could have never been realized using Classical Physics. To probe the characteristics of atoms, nuclei and particles we need comparatively high energies as used for the ordinary life objects. Extensive research is going on in this area but still much is left to be investigated.

While Atomic, Nuclear and Particle Physics are generally separated by different length and energy scales, strong laser fields offer a way to form a bridge among these different areas [1, 2]. From its birth about 50 years ago, Laser Physics has been growing by leaps and bounds. Due to the large progress in high-power laser technology during the last two decades, it is possible today to produce keV photons, MeV ions and GeV electrons by intense short laser pulses ($I \sim 10^{18} - 10^{20}\,\mathrm{W/cm^2}$) which lies far beyond the typical energy scale of Atomic Physics and is more characteristic for Nuclear and Particle Physics. As a consequence, the field of laser-nuclear physics is emerging in recent years [3]. While lasers have always represented important tools for nuclear spectroscopy [4], at present their role is qualitatively changing and growing. Direct or indirect interaction of the nucleus with the laser is quite an interesting field these days both at theoretical as well as experimental level although it is quite challenging. In pioneering experiments, the interaction of intense laser pulses with solid targets has already led to the observation of laser-induced nuclear fission [5], nuclear fusion [6], and neutron production in nuclear reactions [7, 8]. At the moment the most intense laser has an intensity of the order of 2×10^{22} W/cm^2 with a power of 300 TW [9]. The next laser generation aims at phenomena like vacuum polarization and relativistic ion generation [10, 11]. Advanced laser sources might also pave the way to nuclear quantum optics [12, 13] and coherent γ-spectroscopy [14]. The main subject of the present thesis is to concentrate on nuclear probing and excitation using the interaction of strong laser fields with atomic targets rather than solid-state matter. Apart from the achievable high energies, lasers can be utilized in this case to generate well-controlled collisions between atomic constituent particles. The interest thus lies in indirect interactions of the nucleus with an applied laser field, mediated by the

surrounding atomic shells.

Atoms submitted to strong laser fields *e.g.* emit radiation through the ionization-recombination process. Even radiation of a frequency larger than the fundamental frequency of the incoming laser beam can emerge depending upon the energy of the electrons; this process is called high harmonic generation (HHG). This process is being used in this thesis as a tool at the atomic level to find some nuclear signatures.

To obtain the particle recollision energies in the MeV range, there might be different ways to explore the nucleus using atomic techniques under the laser field:

1. to optimize the laser pulse: Klaiber *et al.*, employs specially tailored pulses to counteract the effect of drift and to get the higher harmonics [15] and also Milosevic *et al.*, introduce counter propagating lasers to diminish the drift in order to get high harmonics [16].

2. to change the atomic species: there are some attempts to generate high ponderomotive electrons by using ultra-intense laser light sources, but achieving a high collision yield remains a difficult task due to the drift of electron while recombining. One can think of using high-Z ions [17, 18], but this would in turn reduce the inherent tunneling rate. If we use low-Z ions it would yield enough tunnel ionization, but would not be strong enough to compensate the drift.

   Henrich *et al.*, investigated positronium (an exotic atom which consists of an electron and a positron) in strong laser fields. Under these circumstances, phenomena such as recollisions of electrons and positrons with substantial coherent x-ray generation and gamma ray emission can occur [19]. For this two-body system the tunnel ionization of electron and positron may occur almost oppositely in the laser polarization direction, both experience the identical drift in the laser propagation due to their equal magnitudes of mass and charge. Periodic recollisions occur in spite of the influence of the Lorentz force. Positronium therefore offers interesting prospects for Laser-Particle Physics [20]. Being a purely leptonic system, however, it is not suitable for Nuclear Physics studies, of course.

In accordance with the change of atomic species, this work is based upon the replacement of the electron by a revolving particle outside the nucleus in an atomic bond state. These atoms are called Exotic Atoms: atoms can be formed with other charged particles serving as the negatively charged electrons or the positively charged nucleus. Muons (having 207 times the mass of the electron), pi mesons (having 273 times the mass of the electron), or antiprotons (having 1836 times the mass of the electron) can be substituted for electrons. These exotic atoms exhibit energy levels and transitions similar to ordinary atoms.

Muonic atoms have proven to be particularly useful tools to study the structure of atomic nuclei. In fact, they represent one of the most successful and accurate methods to probe nuclear properties for more than 50 years [21–23]. If we replace the electron by a muon in an ordinary atom then the atom is called a muonic atom. Muons have the same properties as electrons except for:

1. the 207 times larger mass due to which the size of the muonic atom shrinks

2. it is unstable having a life time of 2.2 μsec.

Due to the small Bohr radius of these exotic atoms, the muonic wave function has a large overlap with the binding nucleus. Precision measurements of muonic transitions to deeply bound states can therefore reveal nuclear structure information such as finite size, deformation, surface thickness, nuclear compressibility [21] and polarization. The first X-ray spectroscopy of muonic atoms was performed in 1953 using a 4-m cyclotron [24]. Today, large-scale facilities like TRIUMF (Vancouver, Canada) [25] exist which are specialized in the efficient generation of muons and muonic atoms. New developments aim at the production of radioactive muonic atoms for conducting spectroscopic studies on unstable nuclear species [26]. Muonic atoms, moreover, play a prominent role as catalysts for nuclear fusion [27].

In light of this, the combination of muonic atoms with intense laser fields opens promising perspectives which are investigated in this thesis. Contrary to the traditional spectroscopy of muon transitions between stationary bound states, the exposure of a muonic atom to a strong laser field makes the problem explicitly time-dependent and the muon, thus, a *dynamic* nuclear probe. In this setup, the muon is coherently driven across the nucleus which, for example, gives rise to the emission of radiation and, in general, allows for time-resolved studies on a femtosecond scale. The information on the nucleus gained by laser-assistance can in principle complement the knowledge obtained from the usual field-free spectroscopy of muonic atoms. Against this background, we consider in this thesis the process of HHG from strongly laser-driven muonic hydrogen and deuterium atoms. The process of HHG represents a frequency up-conversion of the applied laser frequency due to a nonlinear coupling of the atom with the external driving field (see [28] for recent reviews). It can be understood within a three-step model, where the bound lepton is liberated from the atom by tunneling ionization, propagates in the laser field, and finally recombines with the core, returning its kinetic energy upon photoemission. Through a comparative study it is demonstrated that the harmonic response from muonic hydrogen isotopes is sensitive to the nuclear mass and size [29]. This shows that muonic atoms subjected to strong laser fields can reveal information on nuclear degrees of freedom. Muonic deuterium molecules in superintense laser fields represent another interesting example towards this combined effort, where field-induced modifications of muon-catalyzed fusion have been investigated [30]. Moreover, muonic hydrogen atoms have been studied as systems which could allow for observation of the Unruh effect [31]. Considering their lifetime, we point out that muonic atoms and molecules may be regarded as quasistable systems on the ultrashort time-scales of strong laser pulses ($\tau \sim$ fs–ps), since the muon life time amounts to 2.2 μs. In a deeply bound state of heavy atoms, the muon lifetime can be reduced to $\sim 10^{-8}$ s due to absorption by the nucleus, which still exceeds typical laser pulse durations by orders of magnitude.

Excitation of atomic nuclei has been one of the major subjects to be investigated by physicists for almost a century. Various mechanisms are capable to change the nuclear quantum state [21]. In particular, transitions between atomic shells can couple to nuclear degrees of freedom. For example, when the energy difference between two atomic states matches a low-lying nuclear transition energy ($\hbar\omega_N \lesssim 100\,\mathrm{keV}$), the energy released dur-

ing the atomic deexcitation can be transferred resonantly to the nucleus leading to its excitation (nuclear excitation by electron transition, NEET) [32,33]. Similar mechanisms proceed via electron capture or scattering [34–36]. Despite their rather small probabilities, these kind of processes are of both fundamental and practical interest since potential applications comprise the efficient triggering of isomeric nuclear states [37] and especially the development of a nuclear γ-ray laser [38].

In the laser field the muonic wave function is oscillating. The resulting time-dependent charge density can lead, for example, to the excitation of the nucleus. Nuclear excitation by the laser-driven surrounding electron cloud has been considered before theoretically [39, 40]. The experimental verification of this process, however, is very difficult [41, 42]. For a muonic atom in a strong laser field the chances should be better due to the small atomic size leading to a large charge density.

To have an idea whether one can observe HHG and the nuclear excitation via laser-muon-nuclear interaction we look at the existing and near-future laser facilities. Several petawatt laser systems all around the world such as HERCULES at the University of Michigan (Ann Arbor, USA) [43], VULCAN at Rutherford Appleton Laboratory (Didcot, UK) [44] or PHELIX at GSI (Darmstadt, Germany) [45]. The next generation of high-power lasers will reach the intensity level of 10^{23} W/cm^2 in the optical and near-infrared frequency range ($\hbar\omega \sim 1$ eV) such as the Extreme-Light-Infrastructure, ELI [10]. At the FLASH facility (DESY, Germany) [46] with a free-electron laser a record intensity of almost 10^{16} W/cm^2 has already been achieved for the VUV frequencies ($\hbar\omega \sim 10 - 100$ eV) and indeed soon they would be able to generate X-ray beams ($\hbar\omega \sim 1 - 10$ keV) at the same place with peak intensities of the order of 10^{20} W/cm^2. Higher intensities could be reachable using plasma surface harmonics to produce ultrashort, high-frequency radiation ($\hbar\omega \sim 10 - 1000$ eV) [47].

Table 1.1: Experimental laser facilities in near future

Range	Laser Photon Energy $[eV]$	Intensity [W/cm^2]
Optical	~ 1	10^{23}
VUV	$\sim 10 - 100$	10^{16}
ultrashort	$\sim 10 - 1000$	
X-ray	$\sim 1000 - 10000$	10^{20}

Thus, our goal is to study nuclear excitation and nuclear properties by virtue of bound muonic motion in an intense laser field. This will extend the well-established studies on muonic atoms (without an additional laser field) and the investigations of laser-nucleus interactions in ordinary atoms. The examinations can also be applied to further exotic systems, like pionic atoms and positronium.

As main results of this thesis, we found that muonic atoms exposed to super-intense laser fields allow for dynamical probing of nuclear properties by the laser-driven muon. Isotope effects are visible in the HHG spectra of light muonic atoms, which can be attributed to the nuclear mass, size and shape. In particular, the harmonic cutoff position depends on the nuclear mass, while the harmonic plateau height is sensitive to the nuclear size

and shape [29]. This opens the perspective to extend the well-established spectroscopy of muonic atoms for Nuclear Physics purposes into the explicitly time-dependent domain via coupling to an ultrastrong laser field. In the cutoff region, coherent hard X-ray photons with energies approaching the MeV range are produced, enabling in principle the generation of sub-attosecond laser pulses for time-resolved nuclear photoexcitation studies. The nucleus can also be excited directly by the laser-driven muonic charge cloud which oscillates periodically across it. For this process of nuclear excitation by coherent muon motion we find very small probabilities, though, because the periodicity of the muon dynamics is far off resonance with the nuclear transition frequency, in general. The frequency mismatch can be overcome in certain cases by utilizing a relativistic atomic beam which effectively enhances the laser frequency through the Doppler shift. Then direct or indirect laser-nuclear excitation becomes feasible.

The thesis is divided to include some phenomena in Laser-matter interaction so to describe tunneling and HHG in **chapter 2**. In **chapter 3**, muonic atoms have been discussed and their importance is highlighted towards nuclear spectroscopy with or without laser field. The relative and center-of-mass motions can be separated in the case of muonic atom since the nucleus is no more an infinitely heavy and pointlike object for the muon. Considering this separation scaling laws are formulated for muonic atoms against the ordinary atoms having electron revolving outside the nucleus. **Chapter 4** targets the role of muonic atoms in probing nuclear signatures when subjected to laser beam. The results for nuclear mass effect and size effects have been discussed first for hydrogen and then hydrogen-like muonic atoms. In **chapter 5** we discuss that Monte Carlo simulations revealing the evolution of the ground state of muonic atom under the influence of a strong laser pulse which leads to the conclusion that muonic atoms oscillate with laser field and can excite the nucleus. The main emphasis is on nuclear excitation via the laser-driven muon revolving around. At the end **chapter 6** provides the concluding remarks with some outlook.

Chapter 2

Laser-Atom Interaction and High Harmonic Generation

2.1 Introduction

Laser Physics came into being in 1960 and after that it progressed very rapidly. Laser beams, containing extremely coherent photons can impart much energy on a certain system to explore it at molecular as well as atomic and even smaller level. Now-a-days physicists are mostly interested in laser-matter interactions apart from the applications of laser in industry. We would concentrate here on laser-atom interactions. With the goal of probing the atomic and nuclear structures, we may also generate short pulses even up to attosecond regime which is somehow one of the reasons to work in one of the applications of laser-atom interaction *i.e.*, High-harmonic generation.

2.2 Multiphoton Ionization

When some energy on an atom is imparted by any means then there are two possibilities for it to absorb the energy:

1. either the energy is taken by the nucleus
2. or the electron goes to some next orbit or leave the bound state

otherwise the energy will not be absorbed. This energy causes to change the atomic potential. It may result into shifting of the electron to some higher orbit and make it loosely bound to the nucleus (excitation) or electron may leave the atom (ionization). In fact, during excitation or ionization, the wave behavior of electron changes due to which its energy eigenvalue changes.

Multiphoton Ionization (MPI) is a transition from a bound atomic state to a free state with the help of multiphotons. The n-photon ionization rate is given by (in perturbative approach)

$$\Gamma_n = \sigma_n I^n \tag{2.1}$$

where n is the minimum number of photons needed for ionization, σ_n is the generalized cross section and I is the intensity of the incident light.

Above-threshold Ionization (ATI) is a multiphoton ionization with the help of more photons than the minimum number of photons required. It is generated by the distortion of atomic potential (the field-induced distortion). After applying the perturbation theory to ATI, above equation can be generalized as:

$$\Gamma_{n+s} \propto I^{n+s} \tag{2.2}$$

where s is the number of excess photons absorbed. This process was verified experimentally in 1982 [48]. The equation describing the photoelectron energy is simply an extension of the Einstein photoelectric effect formula

$$E_f = (n+s)\hbar\omega - E_{ip} \tag{2.3}$$

where n is the number of photons needed for ionization, s is excess photons absorbed and E_{ip} is the ionization potential.

Experiments observed the disappearance of many photoelectron peaks. This peak suppression is obviously non-perturbative as higher-order processes (responsible for the ATI spectrum) have become as important as the lower orders, if not more important. This is a sign of a fundamental breakdown of the perturbative approach.

When a free electron is placed in a laser field, in addition to any translational kinetic energy, a quiver energy due to the oscillatory motion imparted on it by the field. This quiver energy is the so-called ponderomotive energy, U_p, and is given by

$$U_p = \frac{e^2 E^2}{4 m_e \omega^2} \tag{2.4}$$

where e denotes the charge of the electron, E is the local instantaneous electric field, m_e is the mass of the electron and ω is the angular frequency of the electric field.

When the laser field is very intense then it also has a noticeable influence on bound electrons. As Rydberg levels are weakly bound, their induced shifts are very close to the ponderomotive energy, while states comparatively nearer the nucleus have a much smaller polarisability due to which they will be harder to be influenced so they will have a correspondingly smaller shift due to which the shifts of the very low states can be neglected. This means that the ionization potential increases by approximately U_p. At low intensity, N photons are required for ionization, but when the intensity increases, higher states shift by the ponderomotive shift, U_p, so an additional s photons are required for ionization.

We can note an apparent discrepancy in the energies of the emitted electrons as the electron leaves the laser focus it experiences a force, $-\nabla U_p$, due to laser inhomogeneity which is then converted into energy. The electrons gain energy equal to U_p while emerging out

this potential, thus canceling the decrease in energy caused by the increase in the ionization potential. Hence, the photoelectron peaks appear at the same energy as described in Eq. (2.3) regardless of the incident-laser intensity.

In the quasi-classical limit *i.e.*,

$$\hbar\omega < E_{ip} < U_p,$$

an electron acquires its energy in a two-step process:

1. the electron is removed (tunnels) from the primary influence of the atom and then it interacts with the laser field
2. it can be treated classically having two components of the interaction *i.e.*, ponderomotive (quiver) and the drift

For ultrashort pulses, the ponderomotive energy is returned to the wave and it does not contribute to ATI; however, the drift motion remains.

2.3 Keldysh Theory

Let an atom be subjected to a beam and the beam disturbs the atomic potential due to which electron ejects out. Now, if we increase the intensity of the incoming beam, then more electrons will eject even those electrons may also eject out for which the energy will not be enough to leave the atom (potential barrier) that is called tunneling. On further intensity the electrons can easily overcome the attraction of the nucleus to leave the atom.

What would happen if we consider a heavy negative particle instead of the electron in an atom?

The relation that Bohr radius is inversely proportional to the (reduced) mass of the particle in the orbit reveals that the absolute value of potential energy would increase as heavy electron comes closer to the nucleus. It must be noted here that hamiltonians for both the cases would be different. It means that force between nucleus and heavy electron will increase as it is closer to the nucleus and the ionization potential of the new atom will increase means more energy would be needed to eject the heavy particle out. In the presence of the beam we need more number of photons for ionization, so for the same beam which is used for electronic atom we will get multiphoton ionization with the same power law (but with the changed n).

An intense low-energetic (long-pulsed) beam acts like a static field and atomic ionization in this beam will be just like an ionization in static field. The ionization will occur at some threshold value of the field called critical field. Classically, there will be a potential barrier for an electron to move both in atomic and applied static electric fields. A bound electron can tunnel out through this barrier even E (the strength of applied static electric field) is large enough to provide it the energy to overcome the barrier though the tunneling rate is exponentially small if E is small. Ionization, during only a small fraction of the optical cycle, is a characteristic of tunneling, since the probability of overcoming the saddle-point

potential barrier depends very steeply on the field strength. If we increase the value of E, the height of the saddle point decreases. If the value of E becomes equal to critical field E_0, the potential energy becomes equal to the atomic binding energy (E_{ip}) of electron and if E crosses E_0, then ionization over the barrier occurs rapidly. As the field strength is increased the interaction term becomes stronger and gradient becomes more negative. This makes the barrier smaller (suppressed) and in the consequence the ground state does not remain bound any more and the initial wavepacket is free to escape from the atomic potential. This is known as over-barrier ionization (OBI).

The simplest model of tunneling ionization consists of a one-dimensional (1D) Coulomb potential. In an external, static electric field, an electron in this 1D atom sees a finite potential barrier to ionization whose width and height depends on the strength of the field. The threshold intensity for over-barrier ionization is defined as the intensity at which the potential barrier is reduced to the ionization potential of the atom. It can be written as:

$$I_{\mathrm{OBI}} = \frac{cE_{ip}^4}{128\pi e^6 Z^2}. \tag{2.5}$$

Equivalently, over-barrier laser electric field strength is

$$E_0 = E_{\mathrm{OBI}} = \frac{(\alpha Z)^3 m_e^2 c^3}{16e\hbar}. \tag{2.6}$$

Now, if E is below E_0, obviously no over-barrier-ionization is possible rather there will be a tunneling through the barrier (it is only possible when the tunneling time is short compared to the cycle time so that the oscillating field remains a static field for this process. Ionization may proceed over many cycles and also ionization time is longer than the tunneling time.). That is why Keldysh considers the tunneling time and the cycle time and takes their ratio as an important parameter known after him as Keldysh Parameter [49]:

$$\text{Keldysh Parameter } (\gamma) = \frac{\text{Tunneling time } (t)}{\text{Cycle time } (t_0)}$$

If E increases, γ is decreased which leads towards tunneling. For high frequency (short pulsed) beam we need comparatively higher intensities for tunneling. At very low frequencies (long pulsed) tunneling may commence at very low field strengths. A particle needs more time to tunnel through the barrier when the energy of wave packet increases.

If the pulse duration of the ionizing radiation is short compared to the time for the photoionized electron to escape the interaction volume, there is no time for the photoelectron to accelerate before the pulse leaves. The electron drifts in a direction perpendicular to the field in which it was released.

Once free of the potential the electron acts as a classical point charge in a laser field with a certain initial velocity and direction determined by the phase of the field. This means that ionization takes place very rapidly and over a small part of each optical cycle near the peak of the pulse, where the barrier suppression is the greatest. Tunneling ionization has been treated quantum mechanically with the final state being a Volkov state [50] rather than a free, plane wave state for the outgoing ionization.

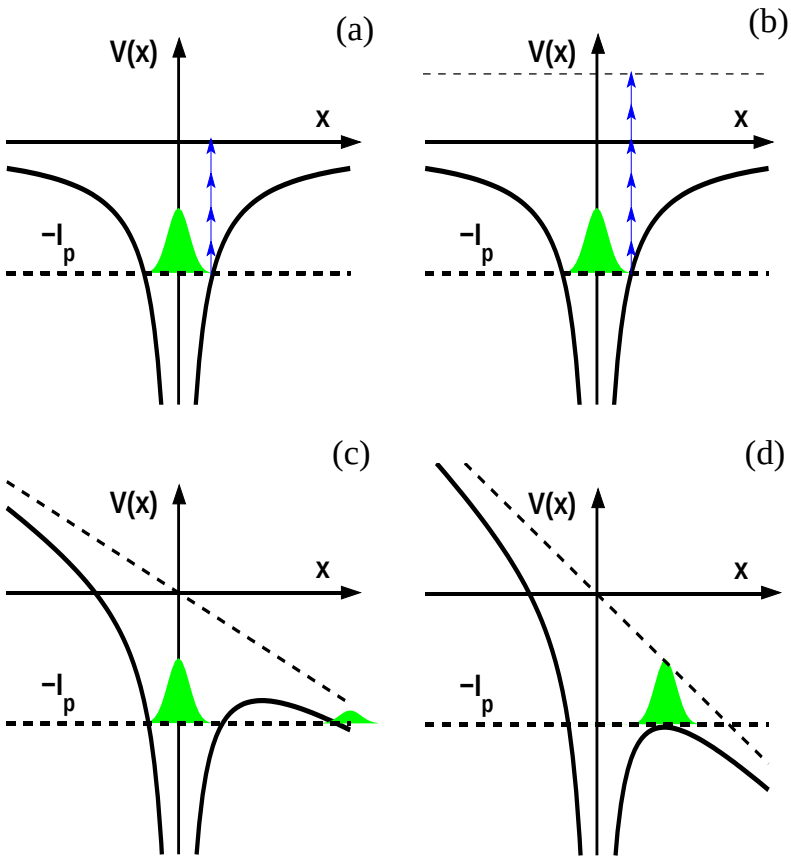

Figure 2.1: The comparison of (a) MPI, (b) ATI, (c) tunneling and (d) OBI is shown.

If the electron comes out of the barrier, it will almost be at rest and its whole potential energy (in the form of ponderomotive potential) will be converted into kinetic energy

$$E_{ip} = \frac{1}{2} m_e v^2, \tag{2.7}$$

the tunneling time will be

$$t = \frac{m_e v}{F} \tag{2.8}$$

where $F = eE$ is the force on the electron and the cycle time is

$$t_0 = \frac{1}{\omega} \tag{2.9}$$

using Keldysh Parameter yields

$$\gamma = \left(\frac{E_{\mathtt{ip}}}{2U_{\mathtt{p}}} \right)^{\frac{1}{2}}. \tag{2.10}$$

This relation tells that for tunneling Keldysh parameter will come out to be less than one $\gamma \ll 1$ and for MPI $\gamma \gg 1$ corresponding to low laser intensity.

This model has two defects which partially cancel each other, resulting in a fairly accurate prediction of I_{OBI}. When the barrier is lowered to the ionization potential, the barrier is completely removed, producing ionization rates of the order of 10^{16} sec^{-1}. These rates are much higher than the threshold rates, and thus overestimate the values for the threshold ionization intensities. (In three dimension it gives the underestimation as barrier is lowered in one dimension only and in every other direction the potential will be higher).

In the long pulse regime, experiments show that the number and the peaks of electron spectra, their angular distributions, and the peak widths all depend upon the intensity of the ionizing radiation; however, the kinetic energies of the electrons are almost independent of the intensity. This independence arises from the nearly complete cancellation of the increased ionization energy of the atom at the time of ionization and the kinetic energy gained by the electron from ponderomotive acceleration as it leaves the interaction volume.

An atom in an intense low-frequency (long pulse) radiation field experiences an ionization potential increase equal to ponderomotive potential (U_p). A photoelectron that would have kinetic energy $E = E_0$ in a weak field is instead produced in an intense field at kinetic energy $E = E_0 - U_p$. The kinetic energy of the newly created photoelectron in the optical field at the same location is also U_p. Thus for long pulses, the electron converts the ponderomotive energy into kinetic energy as it exits from the interaction volume, just compensating for the decrease in its initial kinetic energy due to the raised ionization potential. Because of this conservative nature of the ponderomotive potential, it has been virtually impossible to observe the effects of the ionization potential shift on the energy spectra in long-pulse ATI experiments. The ponderomotive potential, itself, can be clearly discerned by its effect on the electron momenta.

Now, what happens with our heavy electron? Obviously as mass and ionization potential increase in this case so γ will also increase which will not favor the tunneling. Now if we

increase the intensity (E will increase), γ will decrease that favors the tunneling. But it is not the case as we have some scaling rules (discussed in chapter 4) and by applying these rules we are left with unchanged γ.

It must be noted here, that these gammas will be equal and give the same physical results but with the corresponding quantities of applied electric field, intensity of laser beam, the frequency of laser beam etc. So, to get the same amount of ionization the intensity will be shifted to about 10^{22} W/cm^2 for the heavy electron of about 200 times massive that of electron (like muon which is 207 times massive as compared to electron).

Also, as the ionization potential is greater so to get the same γ (for the respective intensity for muonic atom to get the ionization or tunneling), the ponderomotive potential will also be increased. When this massive and energetic particle will strike the nucleus back on its oscillating path it may start nuclear reaction and the energy calculated by Corkum *et al.*, lies in the range to start even nuclear fusion [16].

2.4 High harmonic generation (HHG)

In an intense laser pulse electron wave packet goes away from the atom with the laser field and when the pulse changes its direction, the wave packet returns and may cause certain phenomena:

1. the returning wave-packet may collide with the bound electron to eject it out of the atom. This phenomenon is called non-sequential double ionization.
2. the returning electron may elastically scatter from the nucleus. This phenomenon is called high-order above threshold ionization.
3. the recollision due to the ionization-recombination process of electrons [51, 52] may also generate radiation. Even radiation of a frequency larger than the fundamental frequency of the incoming laser beam may emerge depending upon the energy of the electrons. If the frequency of the emitted radiation is an integral multiple of the fundamental frequency of the laser beam, these higher frequency modes are called harmonics. This phenomenon is called high harmonic generation (HHG).

2.4.1 HHG spectrum

The radiation emitted as a result of recollision process is described by the dipole acceleration $\mathbf{a}(t)$ of the electronic wave function. It can be calculated with the help of Ehrenfest's theorem in the form of a time-dependent expectation value

$$a(t) = \frac{e}{m_e}\langle\psi(t) \mid \bigtriangledown V + E(t) \mid \psi(t)\rangle \tag{2.11}$$

having ψ as the electronic wavefunction with V as a core potential and E is the laser electric field. To obtain the harmonic spectrum, the dipole acceleration is Fourier transformed and can be written as

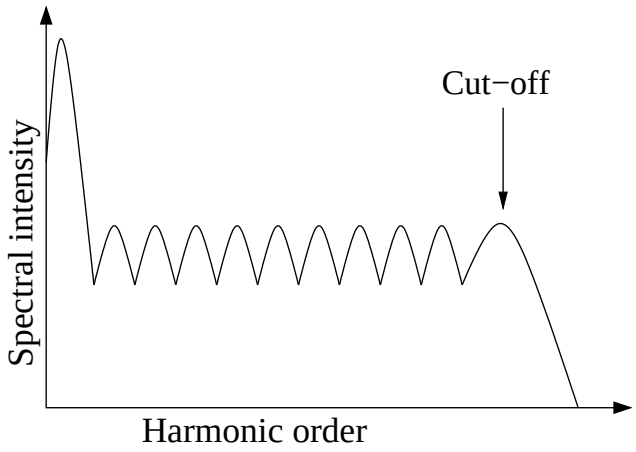

Figure 2.2: Diagram of a typical harmonic spectrum

$$S(\omega) = \mid \int \langle \psi(t) \mid \bigtriangledown V + E(t) \mid \psi(t) \rangle e^{i\omega t} dt \mid^2 \tag{2.12}$$

The above formula shows that the shape of the spectrum would strictly depend upon

- the laser parameters
- the core-potential used.

Fig. 2.2 describes the typical features of HHG spectrum which is drawn in spectral intensity versus the harmonic order, where the ratio of the generated radiation frequency to the laser frequency is termed as the harmonic order. The spectrum has maximum value as its first peak, which is the first harmonic of laser frequency which follows a number of peaks (harmonic orders) as a plateau of constant spectral intensity. Then comes a sharp cut-off at certain harmonic-order.

2.4.2 Three-step model

The scheme of generation of high harmonics can be well understood by a so-called three-step model [51–53]. The three steps are:

1. a part of wave function of electron tunnels through the potential barrier when the atom is subjected to a laser field.
2. this part of wave function is accelerated by the laser beam in the continuum with the laser pulse.
3. once the laser field changes its sign it brings the wave-packet back to the parent ion and recombination occurs to an atomic ground state which yields a photon of high-energy called high harmonic generation.

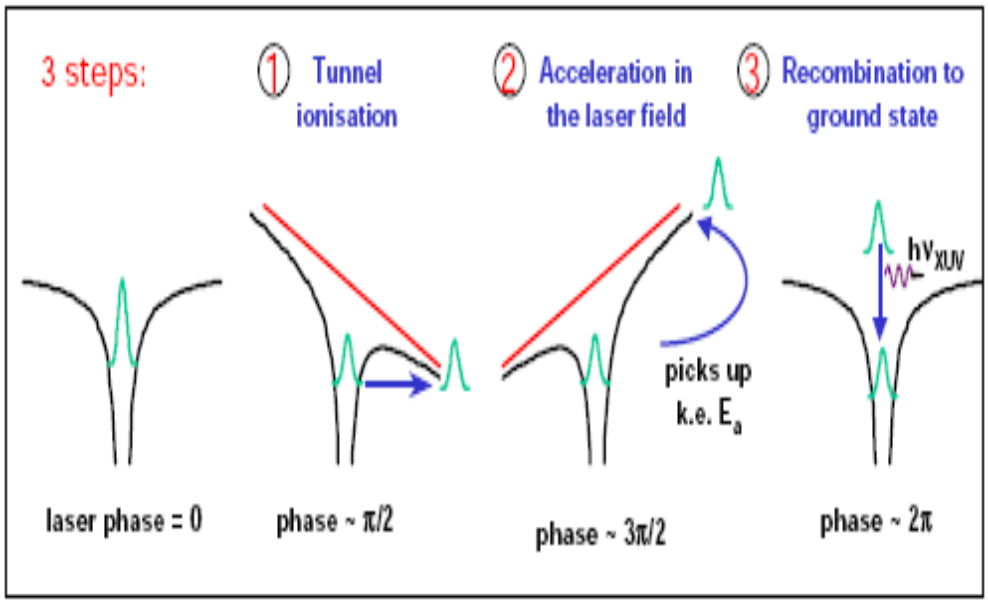

Figure 2.3: Schematic diagram of three-step model

These three steps are depicted in a schematic diagram in Fig. 2.3. According to this model, the maximum photon energy which can be obtained from HHG process is

$$\hbar\omega_{max} = E_{ip} + 3.17U_p, \tag{2.13}$$

having E_{ip} as ionization potential of the target atom and U_p the ponderomotive energy of the electron in the driving laser field (see Appendix A).

2.4.3 Applications of HHG

HHG in noble gases [54, 55] is a promising source to generate coherent XUV (extreme ultraviolet) radiation. It has opened the doors to research fields like XUV nonlinear optics [56] and atto-second pump-probe spectroscopy [57]. Coherent high-harmonic radiation obtained to the X-ray regime has numerous applications in high-resolution spectroscopy and diagnostics [58]. Since the kinetic energy of the emitted radiation of a particle increases with rising incident laser intensity, ultraintense laser pulses have become very important to work with [59–62]. Much has been studied on harmonic generation [2] as far as electronic atoms are concerned. In short, HHG process is considered one of the best ways to produce

- short-wavelength radiation (coherent soft or even hard X-rays) [1]
- attosecond pulses

[1] record of 1 keV [63]

The cut-off formula (2.13) reveals that to obtain the maximum energy of emitting radiation the source must be having

- greater potential energy
- greater ponderomotive energy (means greater laser intensity)

To meet the above two conditions simultaneously highly charged ions are considered to be the best source since they can withstand ultra-high intensities.

The main limitation for HHG is that the free electron generates the out of phase harmonic field [56]. If this dephasing problem can be overcome, we can in principle generate even shorter wavelengths, i.e., more energetic radiation. Also, there is still a clear lack for an efficient system where radiation pressure does not induce substantial ionization in the laser propagation direction and thus reduces coherent high-frequency generation. One can think of the well-known three-step model for single-atom ionization-recollision dynamics [51,53]. But at large laser intensities magnetic field effects come into play and these effects tend to stop the recollision of the electron with its parent ionic core by inducing a considerable drift in laser propagation direction.

2.5 Strong-field phenomena at very high intensities

At even higher laser intensities, the driven motion of free electrons becomes relativistic. This occurs in optical or near-infrared laser fields ($\hbar\omega \sim 1$eV) at intensities above 10^{18} W/cm^2 where the value of the laser vector potential approaches or exceeds the electron rest mass. Typical strong-field phenomena at relativistic laser intensities are non-linear Compton scattering and electron-positron pair creation from vacuum.

Compton Scattering

When the laser intensity is large enough, the Compton scattering acquires essentially a multiphoton character. N photons at frequency ω are absorbed simultaneously by an electron in a single scattering act with emission of one photon at frequency $N\omega$ [64].

Electron-positron pair production

The possibility of using ultra-strong laser fields to create pairs of charge particles (electrons and positrons) has been discussed in the literature [2]. Electron-positron pair production might be possible either in vacuum or indirectly from relativistic electrons accelerated by the ultra-strong laser field. The pair energy $2m_0c^2$ should be of the order of the laser potential energy difference across one Compton wavelength of an electron. Numerically, this is a laser intensity of 10^{30} W/cm^2. That makes the vacuum pair production by pure laser light unobservable with present-day ultra-high-intensity lasers. However, a

particular mechanism of laser-induced pair production (the so-called non-linear Breit-Wheeler process) has been verified in a pioneering experiment at SLAC (Stanford, USA) [65], where a 46 GeV electron beam was brought into collision with an intense optical laser pulse of 10^{18} W/cm^2. After Lorentz transformation to the projectile rest frame, the laser intensity is efficiently enhanced by 10 orders of magnitude and pair creation via few-photon absorption takes place.

On the other hand, pair production from the relativistic electrons generated from the laser focus could have an observable probability at laser intensities of the order of 10^{19} W/cm^2. When the electron energy exceeds the pair production threshold $2mc^2$, the fast electron can produce an electron-positron pair by scattering in the Coulomb potential of a nucleus [66, 67]. Because the pair production threshold is twice the rest energy, the electron motion must be treated relativistically.

Chapter 3

Muonic Atoms

3.1 Introduction

If we replace the electron by a muon in an ordinary atom, then the atom is called a muonic atom. Due to the heavy mass the size of the muonic atom shrinks and the smaller Bohr radius of a muonic atom gives rise the possibility to feel the nucleus via the nuclear properties like finite size, deformation, surface thickness, nuclear compressibility and nuclear polarization [21]. We note that the muon life time is longer as compared to the time period of the laser pulses. Muonic atoms have ever since been useful tools for nuclear spectroscopy (without additional laser fields) due to their compactness. By exposing muonic atoms to strong laser fields we can dynamically probe the nucleus at the atomic scale. To have an idea for the laser parameters required to influence the muonic atoms we take muonic hydrogen as an example. The nuclear Coulomb field experienced by the muon in muonic hydrogen amounts to 2×10^{14} V/cm corresponding to the intensity value of 4×10^{25} W/cm^2. The Bohr radius amounts to $a_\mu = 285$ fm and the binding energy is 2.5 keV.

3.2 Formation of a muonic atom

Naturally occurring atoms have electrons revolving around the nucleus. To form muonic atom, first of all we will have to create the muon. To produce muons, first of all fast pions are produced in an inelastic scattering of high-energy protons:

$$p + p \rightarrow \begin{cases} p + p + \pi^- + \pi^+ + Q_1 \\ p + n + \pi^+ + Q_2 \end{cases} \tag{3.1}$$

where Q_1 and Q_2 are the amounts of energies released during the scattering. With the help of an electromagnetic field the pions are separated from the beam that decay into muons via weak interaction. During their flight the negative pions decay in almost 10^{-8} sec into negative muons:

$$\pi^- \rightarrow \mu^- + \nu_\mu \tag{3.2}$$

These muons are separated from the beam via magnetic fields to some target. To guide and focus the fast beam of muons many deflecting magnets of high magnetic strengths are required.

To form a muonic atom the muon should be captured by an atom to any of its Bohr orbits near the nucleus. Since the muons are formed with the energy of several hundreds of MeV, therefore first of all these muons are slowed down such that the muon velocity becomes less than the velocity of valence electrons of the atom. This slow muon is attracted towards the nucleus and enters the atom in almost 10^{-13} sec (for graphite). Since all muonic states are unoccupied so the muon cascades down to the states of lowest energy (14th orbit for muonic atom is already below the K-electron shell). During this transition, from continuum to some of the lower orbits, there might be

1. an emission of Auger electron
2. an emission of electromagnetic radiation
3. an excitation of the nucleus.

In any case the process takes almost 10^{-13} sec which is much less than the muonic life time that is of the order of microseconds. The theoretical prediction of this kind of formation was first introduced in 1947 [68].

As far as the experimental status of muonic atoms is concerned, they have been formed decades ago in a number of experiments in different compounds using the above mentioned method. For example, muon capture was investigated in several compounds by the detection of electron [69, 70].

3.3 Traditional applications of muonic atoms for nuclear spectroscopy

At the borderline between atomic and nuclear physics, muonic systems play a prominent role [23]. Muonic atoms have been representing powerful tools for nuclear spectroscopy for more than 50 years. In fact, while NEET has been measured for the first time in ^{189}Os in the mid/late 1970s [71], with conclusive evidence even only recently in ^{197}Au [72], in muonic atoms the equivalent process was already observed in 1960 [73–76]. Apart from nuclear excitation, bound muons are also able to catalyze nuclear fission [77] and fusion [27] reactions. The muonic atoms have been considered one of the best candidates for nuclear spectroscopy. There are certain features where these atoms have been quite handful since ever [78]:

Reduced mass

The nucleus has no more infinitely high mass as compared to the muon due to which the nucleus also revolves around a common center. This is the center for both the nucleus and the muon which is not the center of the nucleus as is the case in ordinary (electronic) atom. The reduced mass can be written as

$$m_{red} = \frac{m_\mu m_n}{m_\mu + m_n} \tag{3.3}$$

where m_{red} is the reduced mass of the muonic atom, m_μ is mass of the muon and m_n is the mass of the nucleus. This reduced mass is often used in muonic atoms. In the example of muonic hydrogen, we have $m_{red} \approx 186 m_e$ while the free muon mass is $m_\mu \approx 207 m_e$, m_e being the mass of electron.

Nuclear size effect (volume effect)

The size of the nucleus plays an important role when dealing with muonic atoms. In general the ground and excited states of a nucleus do not have equal charge radii. In an excited nucleus the average nuclear radius changes by $\triangle r^2$. This isomeric shift changes the muonic atom level as well. This kind of excited state may be formed while a muon cascades down within the atom. All the effects which are connected with the extension of the nucleus become important in the case of muonic atoms in contrast with the electronic atoms, for example nuclear deformation, nuclear polarization and vacuum polarization.

Nuclear deformation

Usually the nuclei are considered to have spherically symmetric charge distribution. This distribution is described typically with the help of two parameters: half-density radius and surface thickness (Fermi model) which can be determined phenomenologically via cross-sections of electrons. Whereas the accuracy in determining these parameters could be enhanced while measuring the transition energies in various γ transitions. Since many nuclei are not spherical, hence, muonic atoms are useful to measure the deviation from spherical shape dealing with muonic atoms with a better accuracy.

Nuclear polarization

In the presence of the muon which is very close to the nucleus the charge distribution of the nucleus can be so shifted that the nucleus is polarized. To have an idea of the amount of nuclear polarization we take an example of muonic lead. The transition energy from $2p_{1/2}$ to $1s_{1/2}$ in muonic-Pb is of the order of 10 MeV and the nuclear polarization contributes roughly 10 keV.

Vacuum polarization

The effect in the strong electromagnetic field such that a pair of virtual particle-antiparticle is created is known as Vacuum polarization. For example, the Coulomb field of the nucleus may induce a slight separation of virtual electrons and positrons. The electrostatic potential of the nucleus is changed by this process since the particle around the nucleus would be displaced due to the interaction of electromagnetic field. The change would occur at a distance of roughly one Compton wavelength of the particle. In case of muonic atom the muon would spend more time in the region where the electrostatic potential of the nucleus is changed as compared to the time span of electron due to the compactness of muonic atom. Hence the vacuum polarization effect can be examined in muonic atoms with higher probability. This kind of effects have been investigated in number of experiments [69].

3.4 Muonic atoms in laser beams

Though highly energetic lasers are required to influence the muonic atoms even then muonic atoms have been used to study the atomic transitions with the help of laser for years [79]. Also, the muonic atoms can be formed using laser optically pumped vapors [80].

By applying in addition a super-intense laser field, bound muons can serve as dynamical and controlled probes of the nucleus. We note that the muon life time is long as compared to the time period of the laser pulses. In the laser field the muonic wave function will be oscillating. The resulting time-dependent charge density can lead, for example, to the excitation of the nucleus (see Chapter 5). Nuclear excitation by the laser-driven surrounding electron cloud has been considered before theoretically [39, 40]. The experimental verification of this process, however, is very difficult [41, 42]. For a muonic atom in a strong laser field the chances should be better due to the small atomic size leading to a large charge density. Further observables, like the radiation emitted by the laser-driven system, can give information on nuclear properties (e.g., radius and deformation) like gained from the field-free spectroscopy of muonic atoms.

In muonic atoms, the large muon mass can be accounted for by separating the center-of-mass and relative coordinates of motion. By applying scaling laws (length, time, electric field, ionization potential, laser angular frequency) both to the classical equation of motion and Schrödinger equation, these strong-field processes can be considered for the case of muonic atoms.

3.4.1 Separation of Relative and Center of Mass Motion and Scaling of Muonic Atoms

We consider muonic quantum dynamics in the non-relativistic regime described by the time-dependent Schrödinger equation (TDSE). Due to the large muon mass, the nucleus cannot be treated as an infinitely heavy particle and its motion must be taken into account.

Within the dipole approximation for the laser field, the two-particle TDSE separates into center-of-mass and relative motion. By employing a one-dimensional (1D) hydrogen-like model atom (to be justified in Section 4.4 below), the center of mass evolves in time according to

$$i\hbar\frac{\partial}{\partial t}\Psi\left(X,t\right)=\left[\frac{P^{2}}{2M}+(Z-1)eXE\left(t\right)\right]\Psi\left(X,t\right) \tag{3.4}$$

and the relative motion is governed by

$$i\hbar\frac{\partial}{\partial t}\psi\left(x,t\right)=\left[\frac{p^{2}}{2m_{red}}-m_{red}\left(\frac{Z}{m_{n}}+\frac{1}{m_{\mu}}\right)exE(t)+V\left(x\right)\right]\psi\left(x,t\right) \tag{3.5}$$

with $M=m_{\mu}+m_{n}$ and center-of-mass and relative coordinates X and x, corresponding momentum operators $P=-i\hbar\partial/\partial X$ and $p=-i\hbar\partial/\partial x$, nuclear charge number Z, nuclear potential $V(x)$ and laser electric field $E(t)$. Regarding, the effective charge as

$$q_{e}=m_{red}\left(\frac{Z}{m_{n}}+\frac{1}{m_{\mu}}\right)e \tag{3.6}$$

the relative motion can be written as,

$$i\hbar\frac{\partial}{\partial t}\psi\left(x,t\right)=\left[\frac{p^{2}}{2m_{red}}-q_{e}xE(t)+V\left(x\right)\right]\psi\left(x,t\right). \tag{3.7}$$

Equation (3.4) is the non-relativistic Volkov equation for a particle of charge $(Z-1)e$ and mass M. If we restrict ourselves to the case $Z=1$ as the required laser intensities are the smallest then, while the effects of interest are expected to be appreciable. Note that throughout the nuclear chart the largest relative difference among isotopes, both in mass and charge radius, exists between hydrogen nuclei. Also, for $Z=1$ the effective charge would be equal to ordinary electronic charge $q_{e}=e$.

In this situation, Eq. (1) describes free motion of the center-of-mass coordinate which does not generate radiation and can be ignored. The laser field solely couples to the relative coordinate. For $Z=1$, Eq. (3.7) is reduced to the usual Schrödinger equation for a single particle of charge $-e$ and mass m_{red} in the combined fields of a laser and a nucleus. Now, consider hydrogen atoms (Z=1) where the center-of-mass equation (2) simply describes free motion.

$$i\hbar\frac{\partial\Psi\left(X,t\right)}{\partial t}=\left[-\frac{\hbar^{2}}{2M}\frac{\partial^{2}}{\partial X^{2}}\right]\Psi\left(X,t\right). \tag{3.8}$$

Thus, we are only taking into account the equation for the relative motion which in this case reduces to the ordinary Schrödinger equation for a particle of mass m_{red} in a laser field.

$$i\hbar\frac{\partial\psi\left(x,t\right)}{\partial t}=\left[-\frac{\hbar^{2}}{2m_{red}}\frac{\partial^{2}}{\partial x^{2}}-exE(t)+V(x)\right]\psi\left(x,t\right). \tag{3.9}$$

3.4.2 Scaling laws

Some first information on the behavior of muonic atoms in laser fields can be gathered by scaling considerations [81]. Suppose, that we have a hydrogenlike muonic system on one side and an ordinary hydrogen atom on the other side. We do this scaling by considering TDSE in one dimension for point-like and infinitively massive nucleus.

Let us define position and time for electron in terms of the corresponding quantities for muon

$$x_e = Z\frac{m_{red}}{m_e}x_\mu$$

and

$$t_e = Z^2\frac{m_{red}}{m_e}t_\mu$$

respectively. For a bound electron in electric field **E** we have Schrödinger equation in operator form

$$i\hbar\frac{\partial}{\partial t_e} = -\frac{\hbar^2}{2m_e}\frac{\partial^2}{\partial x_e^2} - \frac{e^2}{x_e} - ex_e.E_e$$

substituting the relation for x_e and t_e. Now, the following scaling relations apply:
the scaling of ionization potential

$$E_{ip}^{(\mu)} = \frac{m_{red}}{m_e}Z^2E_{ip}^{(e)}$$

the scaling of electric field

$$E_\mu = \frac{q_e}{e}\left(\frac{m_{red}}{m_e}\right)^2 Z^3E_e$$

the scaling of frequency of laser beam

$$\omega_\mu = \frac{m_{red}}{m_e}Z^2\omega_e$$

where the subscripts μ and e refer to the muonic system and the hydrogen atom, respectively. This means that a hydrogenlike muonic ion in a laser field with the parameters E_μ, ω_μ behaves like a hydrogen atom in a laser field with E_e, ω_e, provided that the Coulomb potential $V(x)$ arises from a pointlike nucleus. The scaling procedure, however, does not account for nuclear parameters, *e.g.*, the finite nuclear size. Evidently, when the transition from a muonic to an ordinary hydrogen atom is performed, the nuclear radius is not to be scaled but remains fixed. Hence, for atomic systems where nuclear properties play a role, not all physical information can be obtained via scaling.

In Chapter 4, we perform the calculations on muonic atoms in the presence of laser field to probe some of the nuclear signatures like nuclear mass and size after separating the center-of-mass and relative motions.

Chapter 4

Muonic Atoms and Nuclear Spectroscopy via HHG

4.1 Introduction

The field-free nuclear spectroscopy of muonic atoms has been an interesting area of research for decades. It is clear from the previous chapter that it needs very high intensities to influence the muonic atom. In near future we will be able to have lasers of such intensities which can be used to study muonic atoms. For this purpose, a theoretical study of certain properties has been made here. The main object in this chapter is to probe the nuclear properties using muonic atoms in laser fields. These signatures, include, for example, the nuclear mass and the size effects that can be studied dealing with the muonic atoms in ultraintense VUV laser fields. High-order harmonic generation spectra of different isotopes have been considered for this very purpose. As far as Schrödinger wave equation is concerned, in ordinary atoms, the nucleus is considered as point-like and infinitely massive as compared to the electron, revolving around it. In case of muonic atoms these assumptions do not work any more for the nuclei of low atomic numbers. The nuclear effects like nuclear mass and size might become prominent in muonic atoms via irradiation spectrum since the tunneled particle recombines with the nucleus to generate high harmonics in laser field and the recombination probability would depend upon the mass and the size of the nucleus. This consideration does not allow us to study the nuclear mass and size effects within a bound state of electron and nucleus.

4.2 Model Potentials

We solve the TDSE in Eq. (3.7) numerically by making use of the Crank-Nicholson time-propagation scheme (see Appendix C). The laser field is always chosen as a 5-cycle pulse of trapezoidal envelope comprising one cycle for linear turn-on and turn-off each. The harmonic spectrum is obtained by taking the Fourier transform of the dipole acceleration according to Eq. (2.11). In TDSE, various model potentials will be employed:

Soft-core potential

The different mass of the nucleus would affect the tunneling and recombination of the muon due to the different momentum and hence a variation is expected in harmonic spectra for different isotopes which gives us an insight to the mass effect. To calculate the possible nuclear mass effect the usual soft-core potential [82]

$$V_s(x) = -\frac{Ze^2}{\sqrt{x^2 + \left(\frac{a_0\rho}{Z}\right)^2}}\,, \tag{4.1}$$

is used to generate HHG spectra, appropriately scaled for the different isotopes of muonic atoms. Here $\rho = m_e/m_{red}$ and a_0 is the Bohr radius of hydrogen atom.

Hard-core potential

Nuclear size effect could also be promising for muonic atoms in laser beam since the tunneled muon has to come back to the nucleus for the generation of high-order harmonics and with the variation of the size of the nucleus the probabilities of the recombinations would be different which could be seen by comparing the spectra of different isotopes having different nuclear sizes. The softcore potential (4.1) cannot accommodate the nuclear radius R explicitly and suggests us to have some other potential. Taking the nucleus as a sphere of uniform charge density within the nuclear radius, the nuclear drop model is used to employ the potential:

$$V_h(x) = \begin{cases} -\dfrac{Ze^2}{R}\left(\dfrac{3}{2} - \dfrac{x^2}{2R^2}\right) & \text{if } |x| \leq R, \\ -\dfrac{Ze^2}{|x|} & \text{if } |x| > R. \end{cases} \tag{4.2}$$

which explicitly takes the nuclear radius into account. For $R \to 0$ the binding energy of the lowest lying state of this potential becomes unphysical [83] that is why, we start our calculation, from a well known process *i.e.*, from the first excited state which has the correct binding energy [83–85]. To study only the nuclear size effect the disturbance from the variation of nuclear mass has been avoided with the help of accordingly scaled frequencies and intensities with $\omega \propto m_{red}$ and $I \propto m_{red}^4$ so that we obtain the cutoff of both the spectra under consideration at the same position.

Gaussian potential

Another possibility to model a nucleus of finite size applies a Gaussian charge density. In fact, light nuclei are often Gaussian shaped to a good approximation [86]. The corresponding electrostatic potential is

$$V_g(x) = \begin{cases} -\dfrac{Ze^2}{|x|}\mathrm{Erf}\left(\dfrac{|x|}{R_g}\right) & \text{if } |x| > 0, \\ -\dfrac{2Ze^2}{R_g\sqrt{\pi}} & \text{if } |x| = 0. \end{cases} \tag{4.3}$$

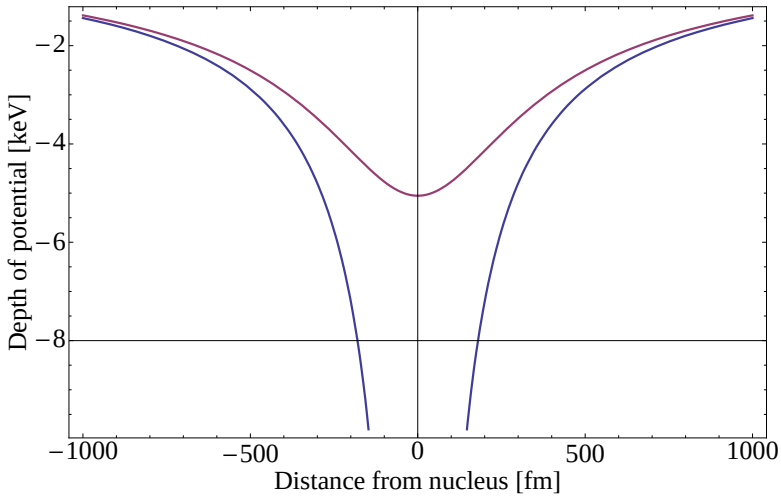

Figure 4.1: The comparison of soft-core (red) and hard-core (blue) potential.

with the error function Erf(z). Both potentials in Eq. (4.2) and (4.3) have only one free parameter, which is connected to the nuclear radius. The relation between the experimentally determined nuclear charge rms radius and the radial parameters in the hard-core and gaussian potentials is given by $R_{\mathrm{rms}} = \sqrt{\frac{3}{5}}R$ and $R_{\mathrm{rms}} = \sqrt{\frac{3}{2}}R_g$, respectively [86]. With the potentials (4.2) and (4.3) we can therefore describe nuclei of the same radius but different in shape. A comparison of the resulting HHG spectra allows for an investigation of the nuclear shape, for this purpose the three potentials are plotted in Fig. 4.1 and Fig. 4.2 where the rms radii are considered for both the hard-core and gaussian potentials given by $\sqrt{\frac{3}{5}}R$ and $\sqrt{\frac{3}{2}}R_g$, respectively.

With regard to the 1D approximation, in general, 1D models are known to retain the essential physical features of nonrelativistic laser-atom interaction for linearly polarized fields [82]; therefore, these models are widely used [87]. Furthermore, in our case the 1D numerics still are a non-trivial task because of the fine grid spacing required to resolve the nuclear extension and the non-standard laser parameters employed. As regards ordinary atoms, the latter would correspond to intense fields in the far-infrared. Eventually, we stress that the goal here is to reveal *relative* differences between physical observables which typically are less sensitive to model assumptions than absolute numbers. The main shortcoming of the 1D approach is the neglect of the ionized muon wave-packet spreading which reduces the total harmonic yield. The spreading of the muon wave packet during a laser period T can be estimated as $\Delta r \sim \Delta v T$ where

$$\Delta v \approx \left(\frac{\hbar e E}{\sqrt{2 m_{red}^3 E_{ip}}} \right)^{\frac{1}{2}}$$

is the velocity width at the exit of the tunnel. In an ultrastrong VUV field ($I = 10^{23}$ W/cm^2, $\hbar\omega = 60$ eV) we obtain $\Delta r \sim 10$ pm, which is by a factor ρ smaller than the spreading of an electron wave packet in an appropriately scaled infrared laser field.

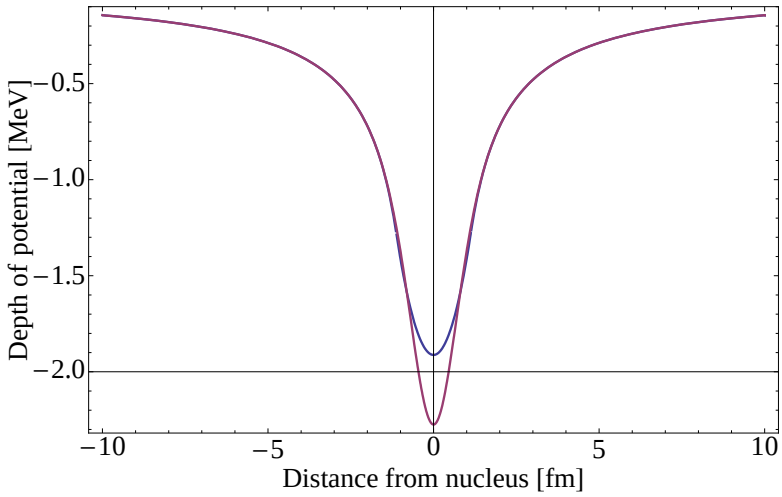

Figure 4.2: Gaussian (red) and hard-core (blue) potentials are shown for hydrogen atom in increasing depth, respectively.

4.3 HHG of muonic hydrogen isotopes

By applying scaling laws (length, time, electric field, ionization potential, laser angular frequency, ionization potential) both to the classical equation of motion and Schrödinger equation, we considered these strong-field processes for the case of muonic atoms. In this way one can easily see that (light) muonic atoms can be ionized by the most powerful present lasers of near-optical frequency or the upcoming X-ray free-electron lasers. Regarding high-harmonic generation, we checked that the known cut-off law for the highest harmonic at a given laser intensity remains true for muonic systems (see Appendix A).

$$E \lesssim E^{\mathrm{OBI}} = \frac{m_{red}^2 c^3}{e\hbar} \cdot \frac{\alpha^3}{16}\,, \tag{4.4}$$

corresponding to the intensity $I^{\mathrm{OBI}} \approx 1.6 \times 10^{23}$ W/cm^2. Here, $\alpha \approx 1/137$ denotes the fine-structure constant. Efficient recombination is ensured if the magnetic drift along the laser propagation direction is negligibly small, which limits the relativistic parameter to [88]

$$\xi \equiv \frac{eE}{m_{red} c\omega} < \left(\frac{16\hbar\omega}{\sqrt{2 m_{red} c^2 E_{ip}}} \right)^{\frac{1}{3}}\,, \tag{4.5}$$

with the atomic ionization potential E_{ip}. We note that condition (4.5) also implies applicability of the dipole approximation. The lowest frequency which simultaneously satisfies Eqs. (4.4) and (4.5) lies in the VUV range and corresponds to $\hbar\omega \approx 27$ eV. At this value, the harmonic radiation has a remarkable maximum energy $\hbar\omega \approx 0.55$ MeV according to Eq. (2.13). Hence, muonic atoms are also promising candidates for the generation of hard X-rays which might be employed to trigger photo-nuclear reactions.

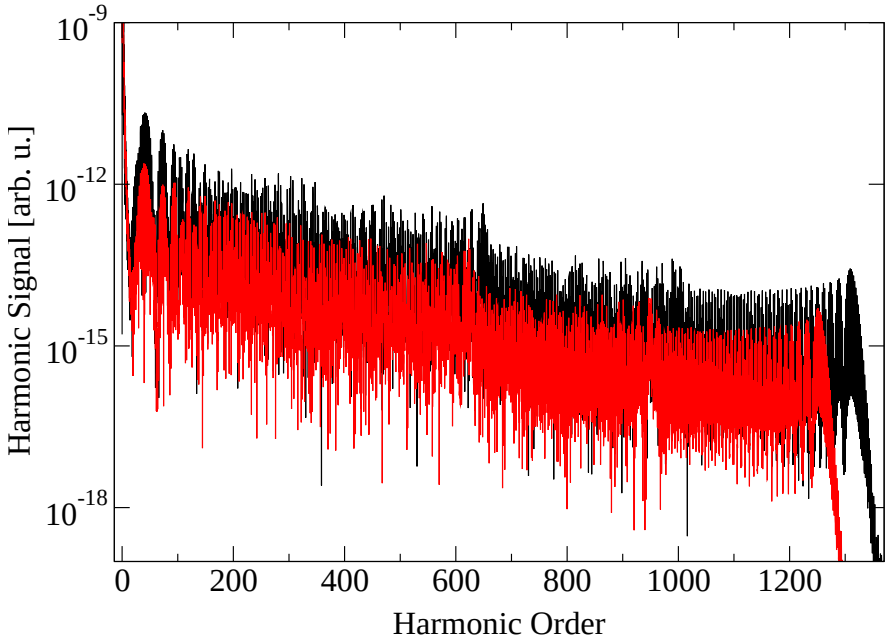

Figure 4.3: HHG spectra calculated with the soft-core potential (4.1). The black and grey (red) lines represent the spectrum for muonic hydrogen and deuterium, respectively. The laser parameters are $I = 1.05 \times 10^{23}$ W/cm^2 and $\hbar\omega = 59$ eV.

4.3.1 Nuclear mass effect

To express the possible effects due to the finite nuclear mass appearing in HHG spectra of muonic hydrogen isotopes, the soft-core potential (4.1) is employed, which is appropriately scaled to the muonic system. Here, we consider only the variation of nuclear mass assuming the nucleus as being point-like. Figure. 4.3 shows the HHG spectra for muonic hydrogen and deuterium in an ultra-strong VUV field of the frequency $\hbar\omega = 59$ eV and the intensity $I = 1.05 \times 10^{23}$ W/cm^2 (similar laser parameters are expected at the attosecond source of ELI [10]). The spectrum of hydrogen is enhanced and further extends by about 60 harmonics. The reason for the spectral enhancement is that the effective particle of the proton-muon system experiences stronger acceleration since it has a smaller reduced mass. The difference in the cutoff position $\hbar\omega = I_p + 3.17U_p$ [28] is also caused by the reduced mass which enters the ponderomotive energy

$$U_p = \frac{e^2E^2}{4\omega^2 m_{red}} = \frac{e^2E^2}{4\omega^2}\left(\frac{1}{m_\mu} + \frac{1}{m_n}\right). \tag{4.6}$$

For the chosen laser parameters we obtain $U_p \gg E_{ip}$ so that the smaller reduced mass leads to a higher cutoff energy. Note that in a situation where $U_p \ll E_{ip}$, the relative order of the cutoff positions would be reversed. Furthermore, we point out that the ponderomotive energy in Eq. (4.6) can be understood as the sum of the ponderomotive energies of the muon and the nucleus. As schematically depicted in Fig. 4.4, both particles are driven into opposite directions by the laser field and when they recollide their kinetic energies add up. In this picture the higher cutoff energy of the hydrogen atom arises from

the larger ponderomotive energy of the proton as compared to the deuteron. Note that the phenomenon that both atomic constituents are driven into opposite directions is most pronounced for positronium, the bound state of an electron and positron [19]. We also observe a few kinks in the spectra of Fig. 4.3. This multiplateau structure is typical of the interaction regime where $\xi \sim 0.1$ (in our case $\xi \approx 0.04$) [28].

At the chosen frequency, the laser intensity assumed in Fig. 4.3 cannot be attained by present-day technology in the laboratory. One might, however, employ a relativistic beam of muonic atoms counter-propagating the laser beam [89]. Then, via the relativistic Doppler shift, the parameters of Fig. 4.3 can be reached by the aid of an intense optical laser pulse of $\hbar\omega \approx 1.5$ eV and $I \approx 6.5 \times 10^{19}$ W/cm^2 at an atomic Lorentz factor of $\gamma \approx 20$. In their rest frame, the atoms would then experience the laser parameters of Fig. 4.3. For muonic hydrogen atoms carrying zero charge, the acceleration cannot directly be accomplished, though. But one could accelerate muons and protons/deuterons separately and let them combine in a merged beams setup. A similar way of producing positronium atoms at $\gamma \approx 20$ via acceleration of negative positronium ions has been proposed recently [90].

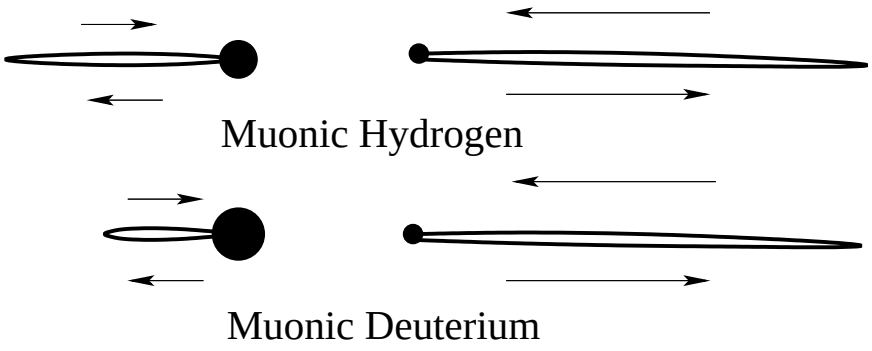

Figure 4.4: Schematic diagram of the motion of the nucleus (on the left) and the muon (on the right) in muonic hydrogen and deuterium in the presence of a laser field polarized in horizontal direction. The oscillation amplitudes are not scaled.

4.3.2 Nuclear size effect

To express the possible effects due to the finite nuclear size appearing in HHG spectra of laser-driven muonic hydrogen isotopes, we need a potential which explicitly takes the nuclear radius into account. We make use of the nuclear drop model, considering the nucleus as a sphere of uniform charge density within the nuclear radius R, and employ the potential (4.2).

Figure 4.5 shows the HHG spectra obtained from the potential (4.2) for muonic hydrogen and deuterium. The proton and deuteron charge radii are $R_p \approx 0.875$ fm and $R_d \approx 2.139$ fm respectively [91]. We note that the overall shape of the harmonic response differs from that shown in Fig. 4.3 due to the different potentials employed. In particular, a dip can be seen at low harmonics ($n\hbar\omega \sim E_{ip}$) followed by a rising plateau region. A similar

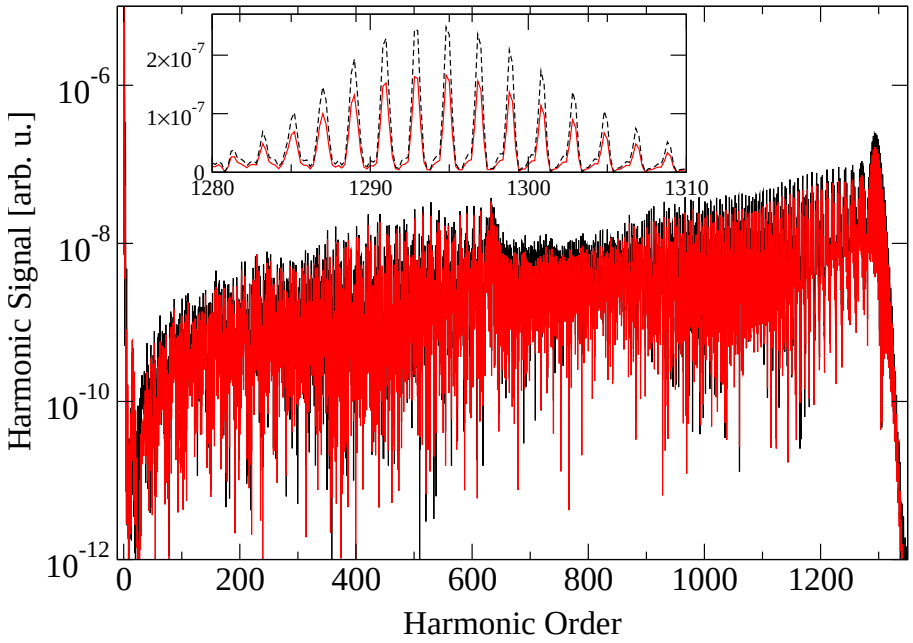

Figure 4.5: HHG spectra calculated with the hard-core potential (4.2). The black line represents the spectrum for muonic hydrogen at the laser parameters $I^{\mathrm{H}} = 1.05\times10^{23}$ W/cm^2 and $\hbar\omega^{\mathrm{H}} = 59$ eV. The grey (red) line represents the spectrum for muonic deuterium at the correspondingly scaled laser parameters $I^{\mathrm{D}} = 1.30 \times 10^{23}$ W/cm^2 and $\hbar\omega^{\mathrm{D}} = 62$ eV. The inset shows a blow-up of the cutoff region on a linear scale, with the black line dashed for better visibility.

feature was found in [92] and attributed to the behavior of non-tunneling harmonics in very steep potentials. More important with regard to the present study is, however, that the harmonic signal from muonic hydrogen is larger (by about 50 % in the cutoff region) than that from deuterium. The reason is that a smaller nuclear radius increases the steepness of the potential near the origin, leading to more violent acceleration and thus to enhanced harmonic emission. With regard to ordinary atoms it has been noticed before that the analytic behavior of the binding potential near the origin is of great importance for the HHG process [85]; according to Ehrenfest's theorem (2.11), the atomic dipole is accelerated by the potential gradient which is largest in this region. In the present situation we therefore find that the plateau height of HHG spectra from muonic atoms is sensitive to the finite nuclear size.

4.3.3 Justification of Dipole approximation

The dipole approximation is justified when the following two conditions are met. First of all, the atomic size must be well below the laser wavelength in order to neglect the spatial dependence of the electromagnetic wave. This is safely guaranteed in our situation: for example in the case of muonic hydrogen, the Bohr radius is $a_\mu \sim 300$ fm while the wavelength of the applied VUV laser field is about 20 nm. The second requirement is

that the muon dynamics is nonrelativistic throughout, so that the laser magnetic-field component may be ignored. This condition is also satisfied here: the muon velocity after ionization is of the order $v \sim c\xi$ with the relativistic parameter (4.5). Despite the ultra-high laser intensities assumed, we always have $\xi \ll 1$ because of the large muon mass and the high laser frequencies (typically $\xi \lesssim 0.1$). This implies moreover, that the excursion amplitude $\triangle X_{exc} \sim \lambda\xi$ of the muon propagating in the field is well below a laser wavelength, *i.e.*, the spatial field variation may again be neglected.

4.4 HHG for muonic atoms with Z>1

So far we have seen the nuclear mass and size effects with the help of muonic hydrogen atoms when they were exposed to VUV laser field. In this section we extend the same business for the low atomic number muonic atoms in ultraintense VUV laser fields. For comparison we also present some more results for $Z = 1$. The main effects in muonic hydrogen versus deuterium have already been demonstrated in the previous section.

4.4.1 Nuclear mass effect

As before, using softcore potential (4.1) we solve the Eq. (3.7) to obtain the dipole acceleration whose fourier transform gives the harmonic spectrum. Since the higher relative mass differences exist for the low atomic number isotopes (as shown in the Table 4.1) in the nuclear chart, the corresponding effect would also be expected to be higher for the light atoms.

Table 4.1: Nuclear masses and sizes of different nuclei

Isotopes	Mass (GeV)	Ref.	Size (fm)	Ref.
H^1	0.9383	[93]	0.875	[91]
H^2	1.8756	[93]	2.139	[91]
He^3	2.8084	[93]	1.9448	[94]
He^4	3.7274	[93]	1.6757	[94]
Be^7	6.5342	[93]	2.2210	[94]
Be^9	8.3928	[93]	2.5180	[94]
O^{16}	14.8952	[93]	2.7013	[94]
Ne^{20}	18.493	[95]	3.0053	[94]
Ne^{23}	21.277	[95]	2.9126	[94]

No doubt the magnitude of ionization potential of muonic atoms is very high but the parameters we use are such that the ratio of E to ω enhances the magnitude of ponderomotive potential such that it supercedes ionization potential and hence the major role is played by U_p instead of E_{ip} to en-shape the spectrum. We look at the Eq. (4.6) describing a ponderomotive energy that consists of two parts: one for the recolliding muon and one for the recolliding nucleus that are driven by the laser field in the opposite directions.

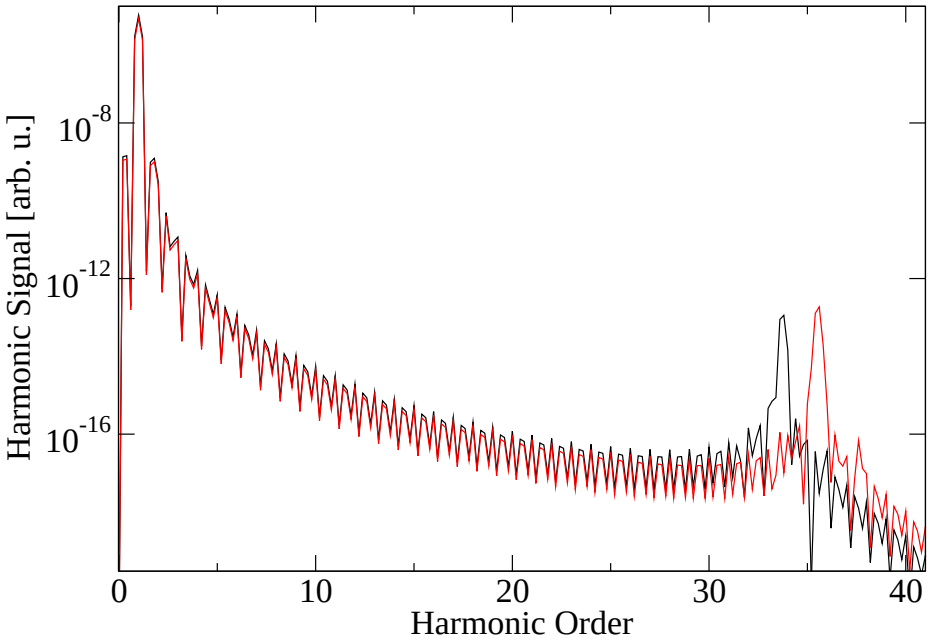

Figure 4.6: HHG spectra calculated with the soft-core potential (4.1). The black and grey (red) lines represent the spectrum for muonic hydrogen and deuterium, respectively. The laser parameters are $I = 1.05 \times 10^{21}$ W/cm^2 and $\hbar\omega = 59$ eV.

From last equations one can expect the cutoff energy to reduce for the heavier nuclei that is confirmed by the spectra shown in Fig. 4.3. Due to the larger reduced mass deuteron-muon system experiences less acceleration compared to the proton-muon system which leads towards the deficiency of the harmonics. Along with this mass effect the cut-off energies are quite appreciable and for this case the photon at the cut-off position has energy $\sim$ 78keV. In this case $U_p >> E_{ip}$ ($U_p \approx 25$ keV and $E_{ip} = 2.5$ keV) but if $U_p << E_{ip}$, the order of cut-off positions for the spectra would be reversed as shown in the Fig. 4.6 where we take the laser with the same frequency but 100 times less intense as compared to that used in Fig. 4.3. Fig. 4.6 describes a spectrum having non-perturbative decay plateau following a large peak at cut-off position. The peak is due to the resonance of the energy of first excited state with the laser energy. We note the reverse order of the cut-off peaks compared to the previous case.

For the parameters assumed in Fig. 4.3, the ratio $\omega/E_{ip} \approx 0.024$ is relatively low. In fact, the same ratio is obtained when an ordinary hydrogen atom interacts with a mid-infrared laser field of frequency $\omega = 0.33$ eV (i.e. $\lambda = 3.7\,\mu$m). Under such circumstances the harmonic signal strength is significantly reduced as compared to HHG in optical or near-infrared fields where typically $\omega/E_{ip} \approx 0.1$ [96, 97]. For this reason we provide in Fig. 4.7 the results for higher driving frequencies. We find here that the strength of harmonic signal improves when we go to higher frequency regime though we do not get high harmonics.

In Fig. 4.8 the harmonic spectra for the isotopes of muonic helium in ultra-intense laser fields are shown. We see that for He^3 the spectrum extends a bit further including 10 more

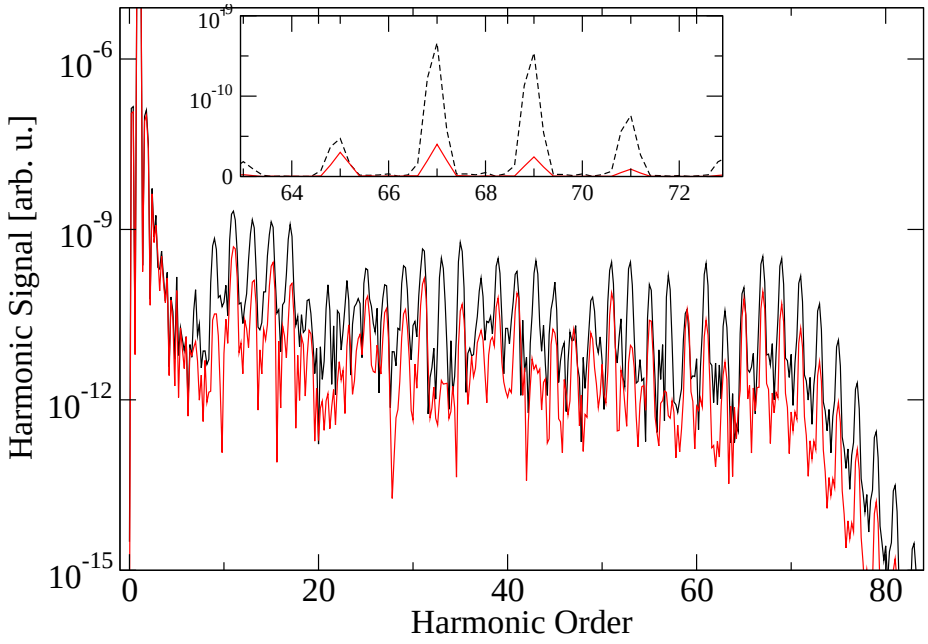

Figure 4.7: HHG spectra calculated with the soft-core potential (4.1). The black and grey (red) lines represent the spectrum for muonic hydrogen and deuterium, respectively. The laser parameters for first case are $I = 1.05 \times 10^{23}$ W/cm^2 and $\hbar\omega = 117.675$ eV and for the second case are $I = 1.05 \times 10^{23}$ W/cm^2 and $\hbar\omega = 176$ eV. The inset shows a blow-up of the cutoff region on a logarithmic scale, with the black line dashed for better visibility.

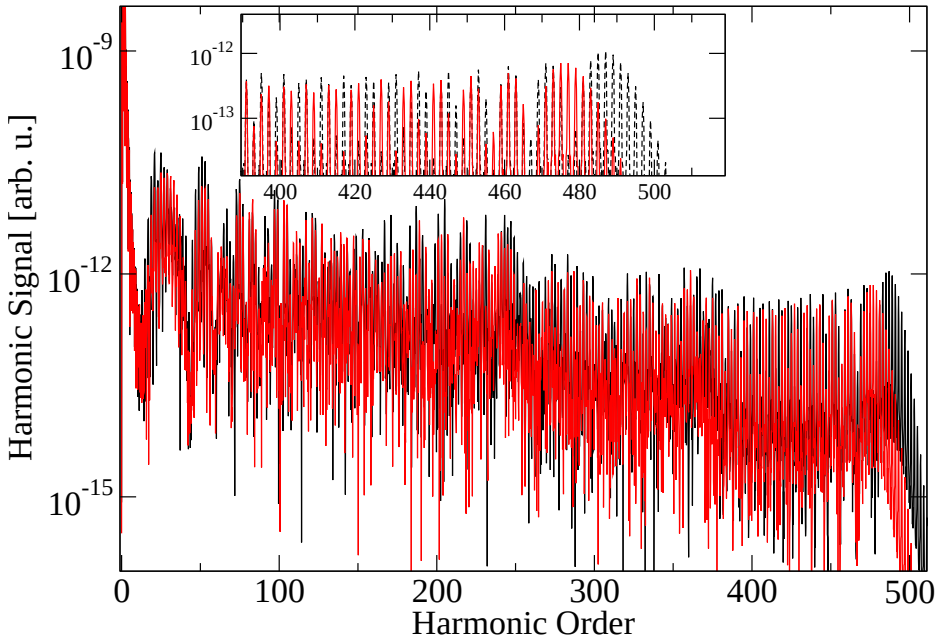

Figure 4.8: HHG spectra calculated with the soft-core potential (4.1). The black and grey (red) lines represent the spectrum for muonic He^3 and He^4, respectively. The laser parameters are $I = 8 \times 10^{24}$ W/cm^2 and $\hbar\omega = 347.2$ eV. The inset shows a blow-up of the cutoff region on a linear scale, with the black line dashed for better visibility.

harmonics in contrast with that of He^4. Formula (4.6) gives us 5 harmonics difference for this case and to justify the extra harmonics the formula (4.6) should be modified since it is for hydrogen only. We have discussed for (4.6) that it is the sum of the ponderomotive energies of the muon and the nucleus and to be the sum ponderomotive potential should then look like

$$U_p' = \frac{e^2E^2}{4\omega^2}\left(\frac{Z^2}{m_n} + \frac{1}{m_\mu}\right) \tag{4.7}$$

which is not the case. The reason is that in hydrogen case center-of-mass does not move with laser field due to its neutrality but in case of $Z > 1$ it moves due to which a ponderomotive potential for center-of-mass comes into play. The ponderomotive potentials for relative coordinates for $Z > 1$ can be written as:

$$U_p^{(r)} = \frac{q_e^2E^2}{4\omega^2 m_r} = \frac{e^2E^2}{4\omega^2}\left(\frac{Z}{m_n} + \frac{1}{m_\mu}\right)^2 \tag{4.8}$$

Moving to the next elements in the periodic table produces minor effects and also the cutoff energies are very small and therefore we just skip them.

4.4.2 Nuclear size effect

There are two methods which we used to study the nuclear size effect:

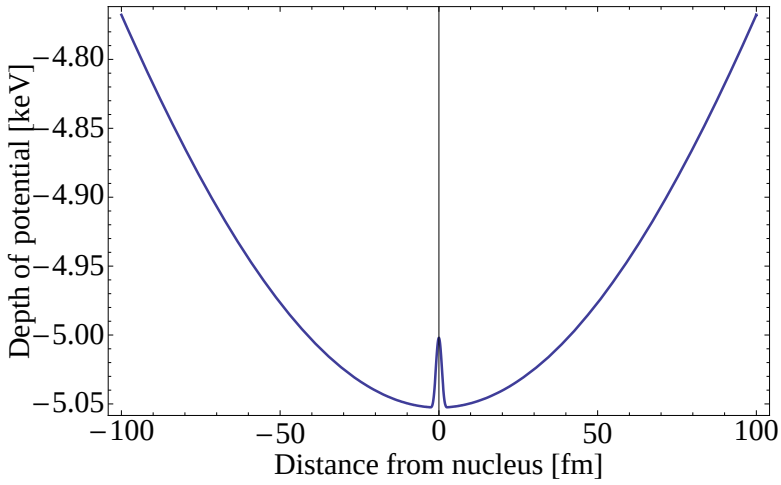

Figure 4.9: The shape of the modified soft-core potential

Modified soft-core potential

Since, the soft-core potential does not accommodate the size of the nucleus explicitly so as a first test we modify the soft-core potential by adding an additional potential to the soft-core potential to include the nuclear size:

$$V_{ms}(x) = V_s(x) + \triangle V\,, \tag{4.9}$$

with

$$\triangle V = \beta \cos^2 \alpha x \tag{4.10}$$

within the interval

$$-\frac{\pi}{2\alpha} \leq x \leq \frac{\pi}{2\alpha},$$

where α and β are scaled with nuclear radius for the right binding energy as

$$\alpha = \frac{\pi}{2R}$$

and

$$\beta = 0.01 \mid V_s(0) \mid .$$

$\triangle V$ is an oscillating potential but we have added only a half period. The comparison of the soft-core (4.1) and the modified soft-core potential (4.9) is shown in the Fig. 4.9.

The results obtained for muonic hydrogen show that this extra factor gives an extra bump of relative height 1% to the soft-core potential of height β (which maybe regarded as negligible) and leads towards the strange shape of the spectrum having an extra dip. The position of the dip shifts towards the cut-off position as the mass of the nucleus decreases. Note that this shape of spectrum is due to the fact that the HHG spectrum mainly depends on the potential used. It is to be noted here that it is an unphysical potential and we applied it just for a test. This test reveals that HHG response is highly sensitive to the potential shape close to the origin.

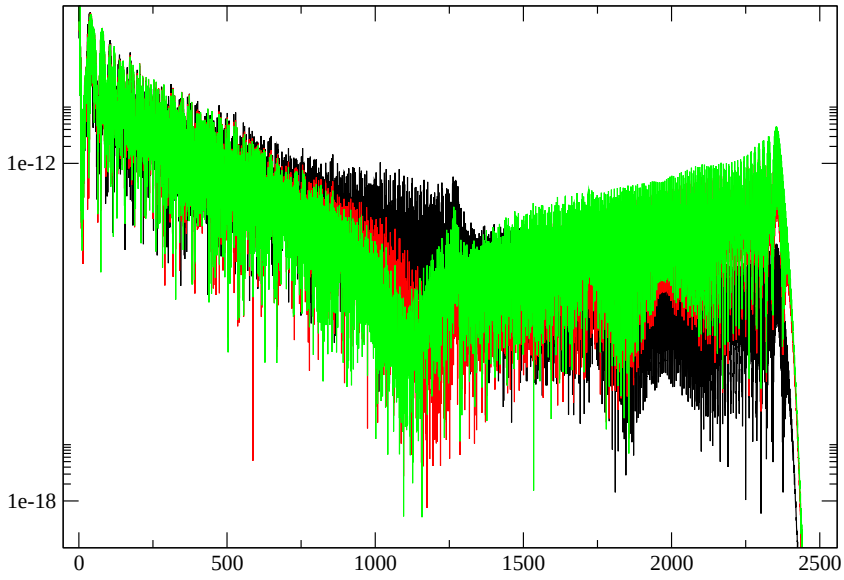

Figure 4.10: HHG spectra calculated with the modified soft-core potential (4.9). The black line represents the spectrum for muonic hydrogen considering nucleus as point-like nucleus, the red line represents the spectrum for muonic deuterium and the green is for muonic tritium.

Hard-core potential

In the second attempt we move towards a physically reasonable potential *i.e.*, the hardcore potential (4.2). It is used to calculate the irradiation spectrum to have an insight on the nuclear size effects. It is a well known nuclear potential considering the nucleus as a uniform sphere.

Since the higher relative size differences exist for the low atomic number isotopes (as shown in the Table 4.1) in the nuclear chart therefore the corresponding effect, would also be expected to be higher for the light atoms.

With the same intensity if the frequency is enhanced three times as used in Fig. 4.10 for both the muonic hydrogen and muonic deuterium then the harmonic signal from muonic hydrogen is larger (by about 52% in the cutoff region) than that from deuterium as shown in Fig. 4.11a.

Keeping the frequency same as for Fig. 4.5, decrease the field strength up to 3.8×10^{22} W/cm^2 for the muonic hydrogen and 4.68×10^{22} W/cm^2 for the muonic deuterium then the cutoff positions further decrease even the harmonic signal from muonic hydrogen remains larger by about 6.58 % in the cutoff region than that from the deuterium as shown in Fig. 4.11b.

In the case of muonic helium the harmonic signal from muonic He^4 should be larger than that from muonic He^3. The difference is observed in Fig. 4.12 of about 11.17 % in the cutoff region. If we further go to muonic beryllium case, the harmonic signal from muonic Be^7 is larger (by about 19.7 % in the cutoff region) than that from muonic Be^9, due to the fact that the latter is bigger than the previous one, as could be seen in Fig. 4.12. The difference in Be is higher than the difference in He since the relative difference in the radii of the corresponding isotopes of Be is higher than that of the isotopes of He. But overall these differences are quite small as compared to H because the difference between the nuclear sizes of the nuclei of isotopes becomes smaller and smaller.

In the case of neon we find the harmonic signal from muonic Ne^{23} is larger (by about 1.61 % in the cutoff region) than that from muonic Ne^{20} as shown in Fig. 4.12c. In case of Helium, Beryllium and so on we need practically no mass effect to compensate since the parameters are almost the same and hence to measure the size effect there would be no need to use two different lasers experimentally.

In order to reveal more systematically the dependence of the nuclear-size effect on the nuclear radius, we have repeated our calculations with the hard-core potential (4.2) within a whole range of radii between 1 fm and 5 fm. The corresponding results of muonic hydrogen + Ne are shown in Fig. 4.13, which displays the percentage relative difference in the HHG plateau height. We emphasize that not all radii considered in this systematic study are realized in nature, of course. For muonic H we observe throughout that the HHG signal decreases the large the fictitious proton radius becomes. This can be understood by the corresponding hard-core potential which becomes less deep, as outlined before.

In the case of muonic Ne, an interesting effect occurs for nuclear radii larger than 3 fm: here the signal strength starts to increase again. The reason for this surprising phe-

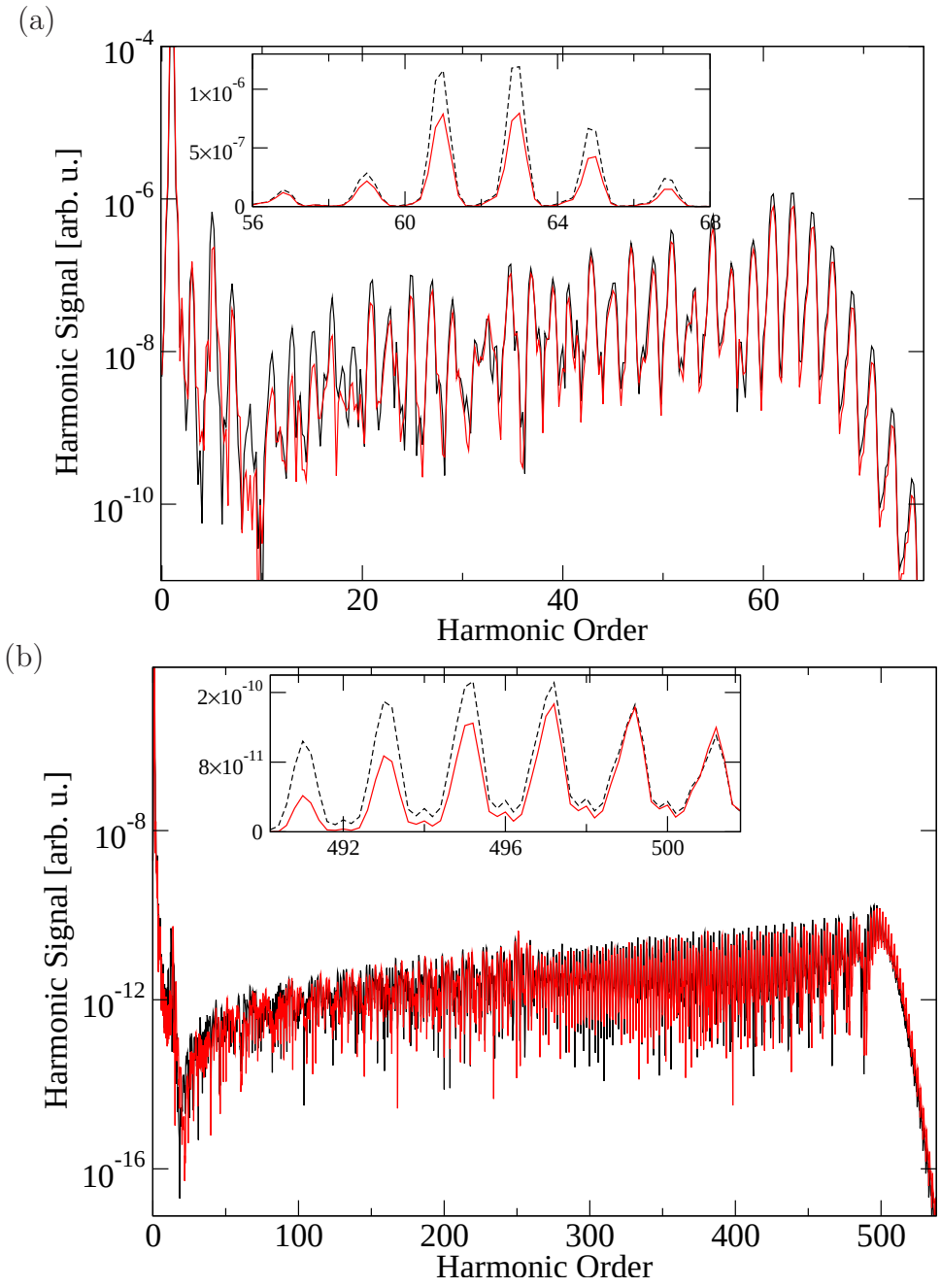

Figure 4.11: HHG spectra calculated with the hard-core potential (4.2). (a) The black line represents the spectrum for muonic hydrogen at the laser parameters $I^{\mathrm{H}} = 1.05 \times 10^{23}$ W/cm^2 and $\hbar\omega^{\mathrm{H}} = 176$ eV. The grey (red) line represents the spectrum for muonic deuterium at the correspondingly scaled laser parameters $I^{\mathrm{D}} = 1.30 \times 10^{23}$ W/cm^2 and $\hbar\omega^{\mathrm{D}} = 186$ eV. (b) The black line represents the spectrum for muonic hydrogen at the laser parameters $I^{\mathrm{H}} = 3.8 \times 10^{22}$ W/cm^2 and $\hbar\omega^{\mathrm{H}} = 59$ eV. The grey (red) line represents the spectrum for muonic deuterium at the correspondingly scaled laser parameters $I^{\mathrm{D}} = 4.68 \times 10^{22}$ W/cm^2 and $\hbar\omega^{\mathrm{D}} = 62$ eV. The inset shows a blow-up of the cutoff region on a linear scale, with the black line dashed for better visibility.

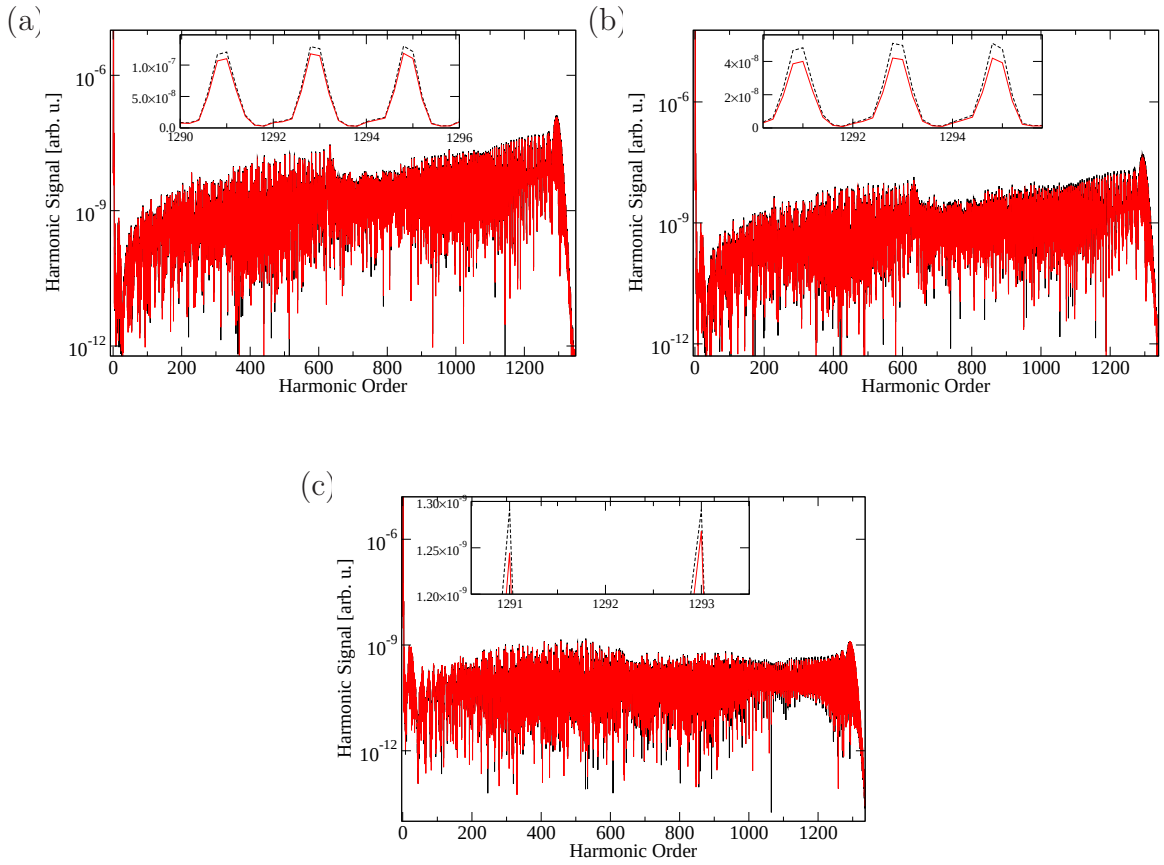

Figure 4.12: HHG spectra calculated with the hard-core potential (4.2). (a) The black line represents the spectrum for muonic He^4 at the laser parameters $I = 8 \times 10^{24}$ W/cm^2 and $\hbar\omega = 347.2$ eV. The grey (red) line represents the spectrum for muonic He^3 at the correspondingly scaled laser parameters $I = 8.3 \times 10^{24}$ W/cm^2 and $\hbar\omega = 350.354$ eV. (b) The black line represents the spectrum for muonic Be^7 at the laser parameters $I = 5.25 \times 10^{26}$ W/cm^2 and $\hbar\omega = 1975.11$ eV. The grey (red) line represents the spectrum for muonic Be^9 at the correspondingly scaled laser parameters $I = 5.32 \times 10^{26}$ W/cm^2 and $\hbar\omega = 1981.9$ eV. (c) The black line represents the spectrum for muonic Ne^{23} at the laser parameters $I = 1.2918 \times 10^{29}$ W/cm^2 and $\hbar\omega = 19554.4$ eV. The grey (red) line represents the spectrum for muonic Ne^{20} at the correspondingly scaled laser parameters $I = 1.3 \times 10^{29}$ W/cm^2 and $\hbar\omega = 19585.4$ eV. The insets show a blow-up of the cutoff region on a linear scale, with the black line dashed for better visibility.

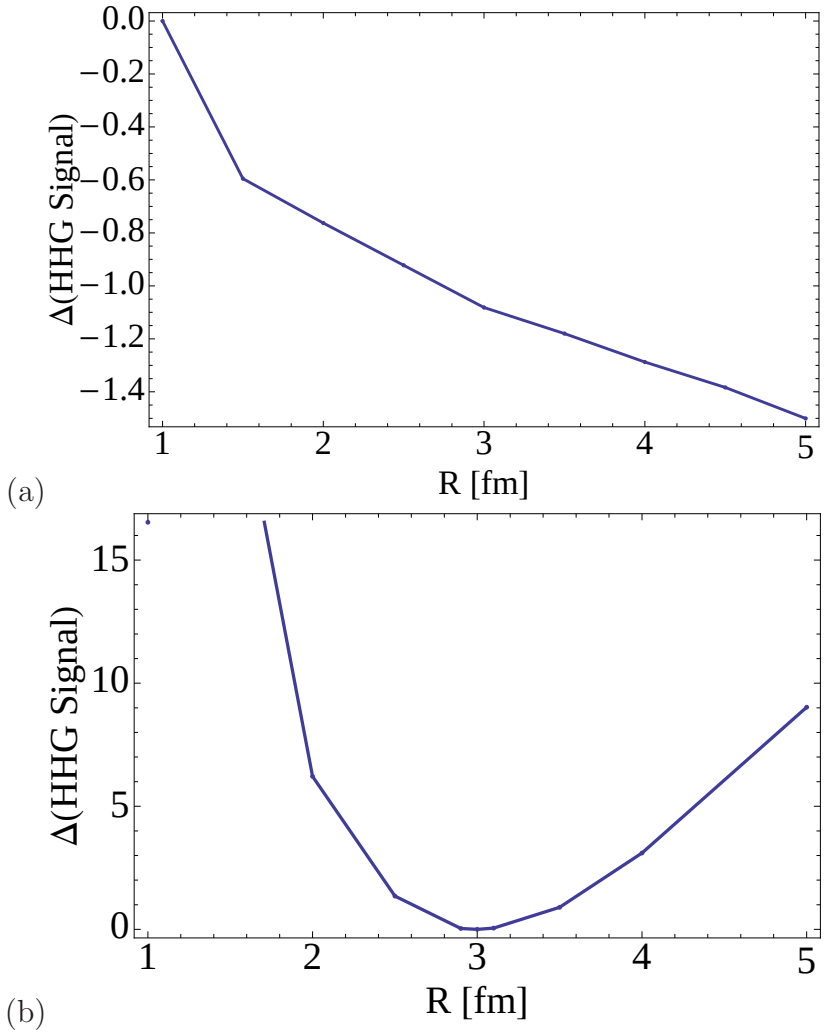

Figure 4.13: Variation of the size for (a) H^1 and (b) Ne^{20} with relative difference of harmonic signal strength at cutoff position with the radius of 1 fm and 3 fm respectively as reference points.

nomenon is that the ionization potential of the muon decreases as the nuclear radius increases. The less tightly bound muon is therefore ionized with higher probability. According to the 3-step model of HHG, this enhances the probability of the whole process. For muonic Ne this effect is dominant and leads to the increasing harmonic signal strength for very large Ne nuclei.

From $R = 3$ fm to 5 fm, there is an enhancement of the ionization probability from 1.95×10^{-8} to 2.57×10^{-6} according to a simple ADK formula.

4.4.3 Comparison with electronic systems

Finite nuclear size effects also appear in high-precision spectroscopic studies of electron transitions in ordinary highly charged ions [98] such as hydrogenlike uranium where the K-shell radius is about 500 fm and the nuclear size $R \approx 7$ fm. In the harmonic signal produced by such systems in the presence of a superintense laser wave, nuclear signatures could be visible, too. It is interesting to compare the expected effects with those found for laser-driven muonic atoms via a simple analysis based on nonrelativistic estimates [99]. Note that our approach to muonic atoms which employs Schrödinger theory is not applicable to highly-charged ions where the bound electron moves relativistically.

In order to draw a comparison, we assume an electronic and a muonic hydrogenlike system of nuclear charge numbers Z_1 and Z_2, respectively, and employ the mass scaling parameter ρ (see above) with $\rho_1 = 1$ for an electronic ion and $\rho_2 \approx 1/200$ for a muonic atom. The K-shell Bohr radius, binding energy, and electric field strength amount to

$$a_K(Z,\rho) = a_0 \frac{\rho}{Z}, \tag{4.11}$$

$$\epsilon_K(Z,\rho) = \epsilon_0 \frac{Z^2}{\rho}, \tag{4.12}$$

and

$$F_K(Z,\rho) = F_0 \frac{Z^3}{\rho^2}, \tag{4.13}$$

respectively, where a_0, ϵ_0 and F_0 denote the corresponding values for ordinary hydrogen. The nuclear radius is approximately given by

$$R(Z) \approx 1.2(2Z)^{\frac{1}{3}}\,\mathrm{fm}$$

and typically varies among different isotopes by a few percent (except for hydrogen vs. deuterium). Similarly pronounced nuclear size effects in the harmonic spectra can be expected when

$$\frac{R(Z_1)}{a_K(Z_1,\rho_1)} \approx \frac{R(Z_2)}{a_K(Z_2,\rho_2)}$$

i.e., when the ratio between the nuclear and the atomic radius which is proportional to $Z^{4/3}/\rho$, has a similar value for both atomic systems. This holds, *e.g.*, for electronic U^{91+} (where $Z_1 = 92, \rho_1 = 1$) and muonic He $^{2+}$ (where $Z_2 = 2, \rho_2 = 1/200$). Consequently, within this simple qualitative consideration we find that the importance of finite nuclear size effects in very heavy electronic systems and light muonic atoms should be comparable. Proposed studies on the harmonic radiation emitted by strongly laser-driven highly-charged ions could therefore aim for detection of nuclear signatures, as well.

One should observe, however, that the binding energy and electric field strength in a highly-charged ion are substantially larger than in a muonic atom when both have the same ratio of $Z^{4/3}/\rho$. *i.e.*, the laser frequency and intensity that must be applied to electronic ions in order to reveal nuclear size effects in the harmonic response need to be larger than for muonic atoms. In this respect, muonic atoms are more favorable systems to study the influence of the nuclear size on the high-harmonic generation process.

4.5 Effects of the nuclear shape

To see clearly the effect of the nuclear shape on the HHG spectrum we consider hard-core potential and the Gaussian potential. We know from the Fig. 4.2 that Gaussian potential is deeper as compared to the hard-core potential within the range of the nucleus. The Fig. 4.14a shows a comparison of the hard-core and the Gaussian potential for muonic hydrogen. The height of the spectrum is depending upon the form of the potential used, the deeper Gaussian potential, leads to an increased height of the spectrum. This behavior is confirmed by Fig. 4.14b where the comparison is taken for muonic oxygen atom. Also, looking at both of the figures one can extract the result that these effects are more pronounced when the size of the nucleus is comparatively smaller.

4.6 Conclusion

As a conclusion, the HHG spectra obtained from the strongly laser-driven muonic atoms reveal some signs of nuclear properties like nuclear mass and size effects. We selected different muonic atoms to study these effects and the results suggest that for the heavy isotopes both the harmonic cutoff and the height of plateau are significantly reduced because they have larger nuclear mass and size due to which they do not get that much kinetic energy to contribute to the harmonic signal as their lighter partners do. With low atomic number atoms, high-energy photons are generated which lie in MeV regime which can ignite the nuclear excitation. For low Z atoms these results can be verified experimentally with the help of near future technology, *i.e.*, by employing intense high-frequency radiation from free-electron lasers or plasma surface harmonics or, alternatively, by combining radiation from existing high-power near-optical laser systems with a relativistic atomic beam. The present study demonstrates that muonic atoms in strong laser fields can be utilized to dynamically gain structure information on nuclear ground states. It also offers the prospect of performing pump-probe experiments on excited nuclear levels since the periodically driven muon can excite the nucleus during one of the encounters and afterwards probe the excited state and its deexcitation mechanism. This laser-induced nuclear excitation process is studied in the following chapter.

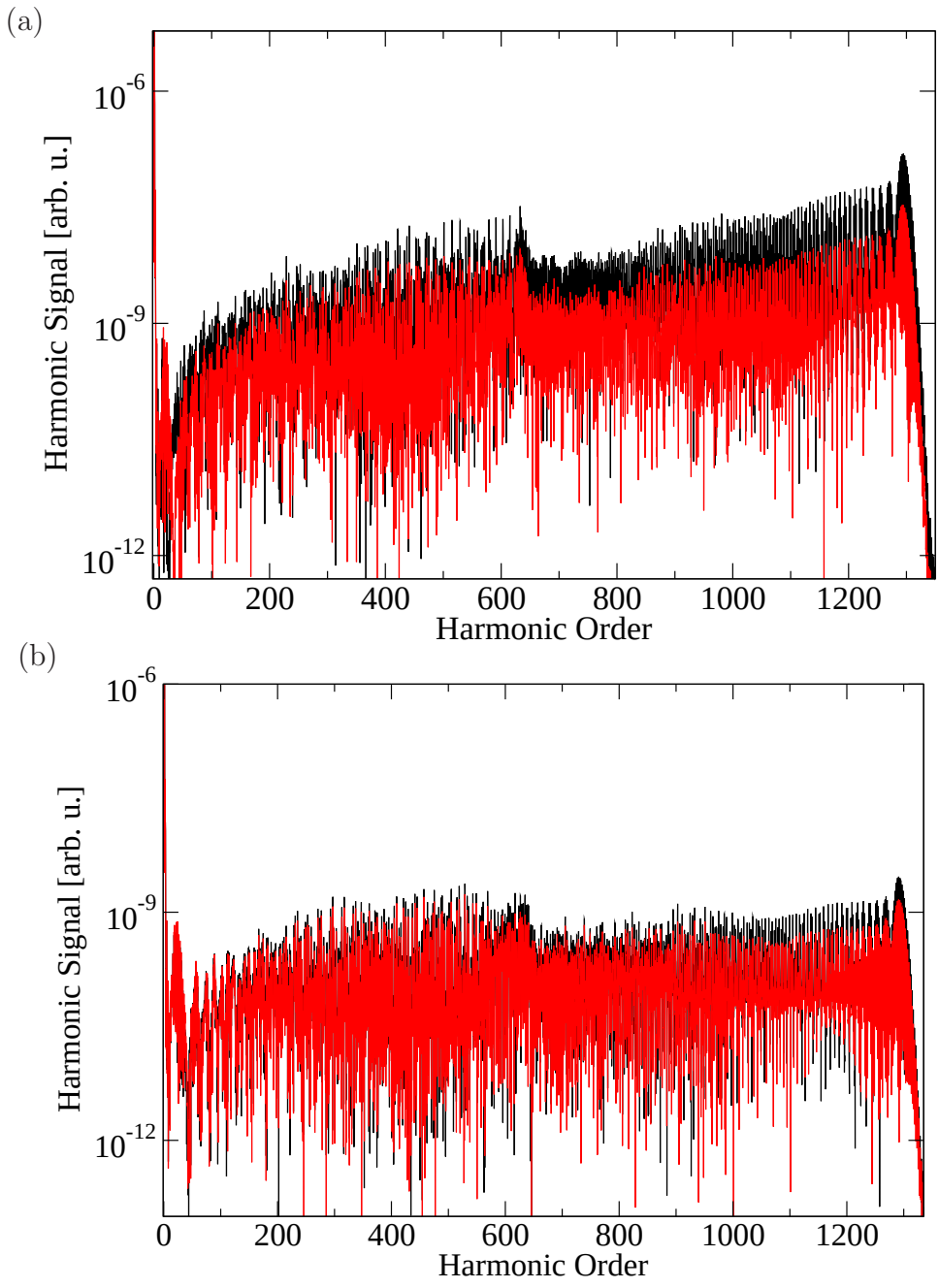

Figure 4.14: (color online). HHG spectra calculated for (a) muonic hydrogen and (b) O^{16} with the hard-core potential (4.2) and the Gaussian potential (4.3) in grey (red) and black lines respectively.

Chapter 5

Nuclear Excitation in Muonic Atoms with Ultraintense Laser Fields

5.1 Introduction

Nuclear excitation has been one of the major subjects of interest for physicists to be investigated for years. At theoretical level certain suggestions and phenomena were introduced, for example, nuclear excitation by electron transition (NEET), nuclear excitation by electron capture (NEEC), photo-excitation, the electron-nucleus scattering and the Coulomb excitation [21]. NEET has been successfully observed in a number of experiments [100, 101] but with very low probability. In NEEC, the predicted excitation rates are small and could not yet be verified in experiments [41] but it has been regarded as the most efficient as far as isomer triggering is concerned [37]. Another example of atom-nucleus coupling is nuclear β-decay into a bound atomic state [102].

Through the field of laser-matter interaction we are now able to examine the laser-nuclear physics at theoretical as well as at experimental level which is otherwise not possible due to the larger wavelength of the laser sources, compared to the nuclear size, available in the laboratories now-a-days, for example, nuclear fission, nuclear fusion, neutron production and nuclear quantum optics [3–8, 12, 13, 27]. Laser-driven collective electron oscillations in a bound state can also trigger the nuclear excitation though not supported by any of the experiments yet [103]. It has been theoretically analyzed [104, 105] a couple of years back but with very less probability. Laser-assisted NEET has also been considered [106] but without any experimental support yet. In the laser induced NEET, Typel *et al.* [107] noticed that the nuclear excitation would be affected by the ionization that is why, we need systems of high binding energies so to afford the high intensities as well and for this purpose the most promising candidates for the nuclear excitation are highly charged ions (HCI). The laser technology has grown quite rapidly soon after its birth even though it would take quite a long to influence the nucleus directly to induce the nuclear excitation due to larger wavelength of photon as compared to the size of the nucleus.

Muonic atoms, being considered one of the favorite systems for nuclear spectroscopy, could also be very useful to investigate the nuclear excitation and also they can survive

higher field strengths (similar as HCI). Muonic atoms have been considered to study a number of nuclear phenomena such as muon-induced fission [77] both at theoretical and experimental level for decades. Also, to investigate the nuclear excitation in muonic atoms is not a new idea rather it has been discussed years back in muon-capture and the transition [108] considering the muon cascading down to the inner orbits. Some theoretical predictions of nuclear excitation were made in the muonic atoms, for example, the dynamic quadrupole interaction between the nucleus and the muon [76] and the resonance mechanism of different mixed states of muonic atoms [109]. The resonance mechanism was supported by experiments though does not hold a complete agreement [110]. Muonic molecules have been considered theoretically in laser beam for nuclear fusion [30] and the atoms for observation of the Unruh effect [31].

5.2 Oscillation of the muon via Monte Carlo simulation

We used classical Monte Carlo simulation techniques to study muon dynamics under the influence of the nuclear Coulomb force and the laser field. Of particular importance are the center-of-mass and relative motion of the muon-nucleus system. Due to the large muon mass, the nucleus should not be considered at rest, as it can be considered in the case of electronic atoms. This fact makes the dynamics of muonic atoms in laser fields especially interesting.

Fig. 5.1 depicts the evolution of the muonic bound state when it is subjected to an intense laser pulse. First of all the ground state is considered without any laser field. When laser is switched on, the cloud shifts with the laser field. Up to half a cycle it continues its motion in the forward direction and after that when the laser field changes its direction, the cloud also moves with it in the backward direction. To make the picture clearer, we take the difference of the position of the cloud with its ground state at different intervals which clearly shows that the muonic charge cloud is driven back and forth along the laser polarization axis. The amplitude of the laser-driven motion is of order of 0.2 times of the Bohr radius of the muonic atom for hydrogen atom. A rough estimate yields that the number is independent of the laser frequency.

The laser-induced oscillations of the muonic charge cloud give rise to the emission of (harmonic) radiation as studied in Chapter 4. Moreover, in our case, the nuclear excitation is caused by laser-driven muon-nucleus collisions.

5.3 Nuclear Excitation by coherent muon motion

Coherent nuclear excitation is calculated in hydrogen-like muonic atoms which are exposed to superintense laser fields. We restrict the consideration to nuclear charges $Z \lesssim 10$ since otherwise the required laser intensities become unrealistically large. Driven by the field, the bound muonic charge cloud periodically oscillates across the nucleus (which we have

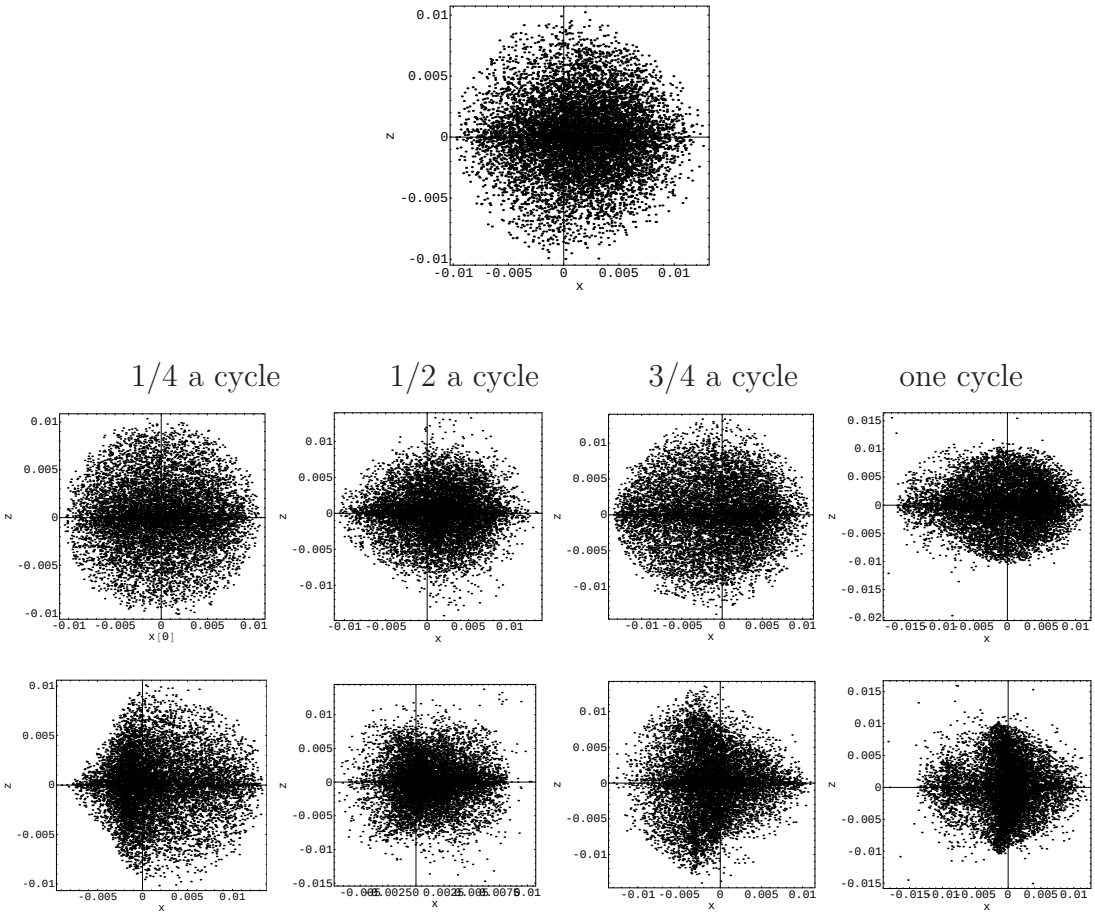

Figure 5.1: Time evolution of the muonic bound state of hydrogen when submitted to an intense laser pulse. The laser is polarized in x-direction and propagating in z-direction. Here, $\hbar\omega = 1.5$ keV and $I = 6 \times 10^{23}$ W/cm^2. The first row is representing the ground state without laser beam. The second row is after shining it with laser and the third row represents the difference between initial and final states.

seen in the last section) which leads to the excitation of the nucleus electromagnetically. In contrast to NEET, this effect does not rely on a resonance condition. It has been studied before in electronic atoms [40, 103, 105, 111], with a focus on the transition to the very low-lying isomeric level in ^{235}U at 76 eV, but the predicted excitation probabilities are small and could not yet be verified in experiment [41, 42]. From the experimental data an upper bound for the excitation probability of $\sim 10^{-5}$ was extracted. We point out that contrary to laser-generated plasma experiments [3], the nucleus is excited solely by its own electron or muon. The process might be called nuclear excitation by coherent electron (muon) motion, NECEM (NECμM). We show that muonic atoms are in principle favorable candidates to observe the effect as the muon produces a much higher charge density within the nuclear volume. The excitation probabilities are always very small, though. We present calculations for nuclear electric multipole transitions as a function of the applied laser frequency and intensity, and discuss the possibility to detect the effect by suitable experimental arrangements.

Hydrogenlike muonic atom in the ground state is assumed which is exposed to an external laser field. The combined influence of the nuclear Coulomb field and the laser field on the muon produces a time-dependent charge density

$$\rho(\mathbf{r}, t) = e^2 |\psi(\mathbf{r}, t)|^2, \tag{5.1}$$

with the muon wave function ψ, which can lead to excitation of the nucleus. The Hamiltonian for the interaction between the muonic and nuclear charge densities is given by [21]

$$H_{\rm int}(t) = \int d^3r \int d^3r_N \frac{\rho(\mathbf{r}, t)\rho_N(\mathbf{r}_N)}{|\mathbf{r} - \mathbf{r}_N|}\,. \tag{5.2}$$

The nuclear long-wavelength limit has been applied here because the nuclear γ-ray wavelength $d = c/\omega_N \approx 10^3$ fm of low-lying transitions is much larger than the nuclear and atomic extensions (r, $r_N \lesssim 10$ fm), where ω_N is the frequency of the nuclear excitation defined as

$$\hbar\omega_N = E_1 - E_\circ \tag{5.3}$$

where $E_\circ$ and E_1 are the ground state and excited state energies of the nucleus, respectively. The nuclear levels are characterized by their total angular momenta I_0 and I_1 and the corresponding projections M_0 and M_1 onto the z-axis. Furthermore, as an initial condition, the nucleus is assumed to be distributed uniformly on the $2I_0 + 1$ degenerate states $\mid I_0 M_0 >$. Then the probability of finding the nucleus in any of the excited states $\mid I_1 M_1 >$ at time t is defined as

$$P_{0\to1}(t) = \frac{1}{2I_0 + 1} \sum_{M_0=-I_0}^{I_0} \sum_{M_1=-I_1}^{I_1} \mid b_1(t) \mid^2, \tag{5.4}$$

where

$$b_1(t) = \frac{1}{i\hbar} \int_0^t d\tau \langle I_1 M_1 \mid V(\tau) \mid I_0 M_0 \rangle e^{i\omega_N \tau}. \tag{5.5}$$

Moreover, since we are interested in electric multipole transitions we neglect the current-current part which would give rise to magnetic transitions. After a multipole expansion of the Coulomb interaction in Eq. (5.2),

$$b_1(t) = -\frac{e^2}{i\hbar}\int_0^t d\tau e^{i\omega_N \tau}\int d^3r \int d^3r_N \frac{\rho(\mathbf{r}-\mathbf{u}(\tau))}{|\mathbf{r}-\mathbf{r}_N|}\rho_{01}(r_N)$$

where

$$\rho_{01}(r_N) = \sum_\sigma < I_1 M_1 \mid \psi^\dagger(r_N,\sigma)\psi(r_N,\sigma) \mid I_1 M_1 > .$$

The probability for an electric transition between the nuclear states $|0\rangle$ and $|1\rangle$ becomes (within the first order of perturbation theory)

$$P_{0\to 1}(E\ell) = \left(\frac{4\pi e}{\hbar}\right)^2 \frac{B(E\ell)}{(2\ell+1)^3}\left|\int_0^T dt\ F_\ell(t) e^{i\omega_N t}\right|^2 \tag{5.6}$$

with the laser pulse duration $T = 2\pi N/\omega$, the nuclear transition energy $\hbar\omega_N$, the multipolarity ℓ, and [105]

$$F_\ell(t) = \int d^3r \frac{\rho(\mathbf{r},t)}{r^{\ell+1}} Y_{\ell 0}(\Omega)\,. \tag{5.7}$$

Here, $Y_{\ell 0}(\Omega)$ is a spherical harmonic and cylindrical symmetry along the z axis is employed. The reduced transition probability $B(E\ell)$ in Eq. (5.6) results from the integral of the nuclear transition density ρ_N over nuclear coordinates in the usual way. Our goal is to obtain a closed-from analytical expression of $P_{0\to 1}(E\ell)$. To this end we follow the model developed in Ref. [105]. We apply the dipole approximation to the laser field

$$\mathbf{E}(t) = E_0 \sin(\omega t)\mathbf{e}_z \tag{5.8}$$

which couples to the muon via $e\mathbf{E}.\mathbf{r}$. This approximation is well justified since the muonic Bohr radius a_0 is much smaller than the laser wavelength, and the laser field strength will be restricted to values where the muon dynamics stays nonrelativistic. Moreover, the binding Coulomb field of the nucleus is modeled by a spherical harmonic oscillator potential

$$V(r) = \frac{1}{2}m\omega_0^2 r^2, \tag{5.9}$$

with the muon mass m and the oscillator frequency ω_0 [105, 112]. This procedure has proved useful for a nonperturbative, though approximate description of the laser-driven dynamics of bound states which otherwise is impossible by analytical means.

When a particle is bound in a harmonic potential the influence of an external laser field can be taken into account to all orders [see Eq. (5.11) below]. It is interesting to note that in the case of muonic atoms the approximation becomes the better the heavier the binding nucleus is because the potential inside an extended nucleus (considered as a homogeneously charged sphere) is indeed harmonic. In very heavy muonic atoms the orbital radius is so small that the muon spends most/half of its time in the nuclear interior.

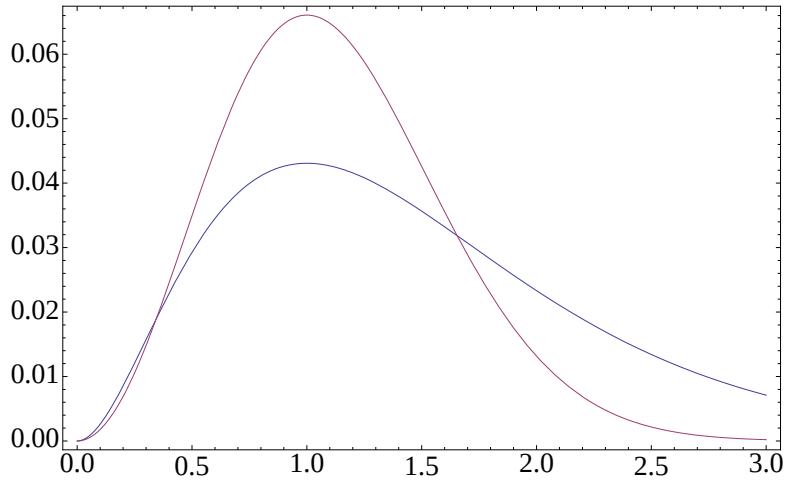

Figure 5.2: Comparison of the ground state wave functions in a Coulomb (blue dashed line) and a harmonic oscillator potential (red solid line). Plotted is $a_0 r^2 |\psi|^2$ versus r/a_0. Both wave functions coincide in their characteristic properties having the same energy eigenvalues and radial peak positions.

However, as motivated before, we will consider light muonic systems where the use of the harmonic oscillator potential clearly represents an approximation only. We stress that this approach is exploited solely to treat the field-induced time evolution of the atomic state; the muonic interaction with the nucleus is correctly described by a Coulomb potential [see Eq. (5.2)]. The oscillator length

$$a_0 = \sqrt{\frac{\hbar}{m\omega_0}} \tag{5.10}$$

is chosen to coincide with the atomic Bohr radius of the muon. With this choice, also the actual binding energy agrees with the oscillator ground-state energy. In Fig. 5.2 the harmonic oscillator ground state is compared with the Coulombic 1s state. Due to the similar shapes of the densities this method allows an order-of-magnitude estimate of $P_{0\to 1}(E\ell)$.

The main physical implication of the approximation is that the muon cannot be ionized since a harmonic oscillator has bound states only. Being interested in nuclear excitation by the laser-driven bound muon dynamics, we therefore restrict the laser intensity to values where ionization may safely be ignored. Nuclear excitation by rescattering of ionized electrons in laser fields has been discussed elsewhere [16, 18, 113]. However, we consider only the nonresonant case where ω_0 is considerably different from ω_N. In this situation the correct atomic level structure is of minor importance. (Note that for $\omega_0 \approx \omega_N$ the NEET process is possible anyway.)

The Schrödinger equation for the muon motion in the combined fields can be solved analytically. Up to an irrelevant phase factor, the muon wave function reads [105]

$$\psi(\mathbf{r}, t) = \phi(\mathbf{r} - \mathbf{u}(t)) \tag{5.11}$$

where

$$\phi(r) = \left(\frac{1}{\pi a_0^2}\right)^{\frac{3}{2}} e^{-\frac{r^2}{a_0^2}}$$

is the ground-state wave function in the harmonic oscillator potential and

$$\mathbf{u}(t) = u_0 \left[\sin(\omega t) - \left(\frac{\omega}{\omega_0}\right)\sin(\omega_0 t)\right]\mathbf{e}_z \tag{5.12}$$

is the periodic displacement caused by the laser field, with

$$u_0 = \frac{eE_0}{m(\omega_0^2 - \omega^2)}.$$

In the limit $\omega \ll \omega_0$ of interest here,

$$\mathbf{u}(t) \approx \frac{eE_0}{m\omega_0^2}\sin(\omega t)\mathbf{e}_z$$

looks similar to the classical trajectory of a free muon in the laser field, but the excursion amplitude is reduced by a factor $(\omega/\omega_0)^2$ due to the harmonic binding force. Eq. (5.11) has an intuitive interpretation of the muon time evolution: the wave packet keeps its shape but is periodically shifted across the nucleus by the driving laser field. With the corresponding charge density $\rho(\mathbf{r} - \mathbf{u}(t))$ the spatial integral in Eq. (5.7) can be solved exactly. For electric dipole, quadrupole and octupole transitions we obtain

$$\begin{aligned}
F_1(t) &= \frac{\sqrt{3}}{2\pi u^2}\left[\sqrt{\pi}\mathrm{Erf}(x) - 2xe^{-x^2}\right] \\
F_2(t) &= \frac{\sqrt{5}}{2\pi u^3}\left[\sqrt{\pi}\mathrm{Erf}(x) - \left(2x + \frac{4}{3}x^3\right)e^{-x^2}\right] \\
F_3(t) &= \frac{\sqrt{7}}{2\pi u^4}\left[\sqrt{\pi}\mathrm{Erf}(x) - \left(2x + \frac{4}{3}x^3 + \frac{8}{15}x^5\right)e^{-x^2}\right]
\end{aligned} \tag{5.13}$$

with the Gaussian error function $\mathrm{Erf}(x)$ and $x = u(t)/a_0$ (as seen in Appendix C). In order to prevent field-induced ionization the laser electric field strength should be far below the barrier-suppression value

$$E_{\mathrm{OBI}} = \frac{(\alpha Z)^3 m^2 c^3}{16e\hbar}, \tag{5.14}$$

where the binding Coulomb potential is suppressed by the laser field all the way to the bound energy level. This implies $u_0 \ll a_0$ (in fact, $u_0 = a_0/16$ at $E_0 = E_{\mathrm{OBI}}$) and the muon velocity $v \sim \omega u_0 \ll c$ remains nonrelativistic. We may therefore perform in Eq. (5.13) a Taylor series expansion in the small parameter x yielding $F_\ell(t) \sim u(t)^\ell$. The time integral in Eq. (5.6) then gives

$$P_{0\to 1}(E\ell) \approx C_\ell\,\alpha^2 \frac{B(E\ell)}{e^2 a_0^{2\ell}}\frac{d^2}{a_0^2}\left(\frac{u_0\omega}{a_0\omega_N}\right)^{2\ell}, \tag{5.15}$$

with the QED fine-structure constant α, the numerical constants

$$C_1 = \frac{128}{81} = 1.58, \tag{5.16}$$

$$C_2 = \frac{2048}{5625} = 0.364, \tag{5.17}$$

and

$$C_3 = \frac{8192}{60025} = 0.136 \tag{5.18}$$

for electric dipole, quadrupole and octupole transitions, respectively, and assuming $\omega_0 \gtrsim \omega_N$. We note that a fast oscillating term

$$\sin^2\left(\frac{1}{2}\omega_N T\right) = \sin^2\left(\pi N \frac{\omega_N}{\omega}\right)$$

occurring in Eq. (5.6) when evaluating the time integral has been averaged over frequency in Eq. (5.15) to produce a factor $\frac{1}{2}$. The reason is that an intense short laser pulse comprises a large frequency bandwidth so that the $\sin^2$ factor will adopt a different value for each spectral component. A $\sin^2$ time dependence is typical for the population dynamics of a two-level system in an external periodic field [103, 114].

The nuclear excitation probability in Eq. (5.15) essentially scales like

$$P_{0\to 1}(E\ell) \propto a_0^{-2(\ell+1)}, \tag{5.19}$$

with the Bohr radius, which clearly demonstrates the expected result that compact atomic states are advantageous. For example, the probability for a nuclear $E1$ transition in a hydrogenlike muonic atom is larger by 9 orders of magnitude than in the corresponding electronic system, when the laser field strength is accordingly scaled so that the ratio u_0/a_0 is identical. Note that

$$B(E\ell) \propto e^2 R_N^{2\ell} \tag{5.20}$$

with the nuclear radius R_N so that a factor $(R_N/a_0)^{2\ell}$ is contained in Eq. (5.15). Apart from this scaling, the atomic size enters through the factor $(u_0/a_0)^{2\ell}$ which depends on the applied laser intensity. The appearance of the ratio u_0/a_0 is intuitive since the larger its value the closer the muon comes to the nucleus, this way increasing the mutual Coulomb interaction. By choosing appropriately large laser fields with

$$E_0 \lesssim E_{\mathrm{OBI}} \tag{5.21}$$

the ratio u_0/a_0 can be optimized to values of several percent. Via the displacement u_0 the excitation probability depends like

$$P_{0\to 1}(E\ell) \propto E_0^{2\ell} \tag{5.22}$$

on the laser field strength. This behavior is reminiscent of multiphoton processes in atoms or molecules which scale as E_0^{2n} when n laser photons are involved. The photon order n formally corresponds to the multipolarity ℓ of the transition here. Within this analogy, the excitation mechanism might be interpreted as 'multiphonon' absorption from the periodically oscillating muon charge density. The main factor, however, determining the absolute value of the probability is the frequency ratio $(\omega/\omega_N)^{2\ell}$. In optical or infrared laser fields the large frequency mismatch suppresses the nonresonant process by many orders of magnitude.

Table 5.1: Parameters of the atomic nuclei under consideration. Given are the electric multipolarity, nuclear transition energy, and reduced transition probability (in Weisskopf units). The last two columns contain the binding energy and Bohr radius of hydrogenlike muonic ^{19}F, ^{16}N, and electronic ^{235}U (treated nonrelativistically). The data are taken from [33, 115].

nucleus	type of transition	$\hbar\omega_N$ [keV]	$B(E\ell)$ [w.u.]	$\frac{1}{2}\hbar\omega_0$ [keV]	a_0 [fm]
^{19}F	$E1$	110	0.0012	228	28.4
^{16}N	$E2$	120	1.7	138	36.5
^{235}U	$E3$	0.076	0.0007	115	575

5.4 Results

Based on Eq. (5.15) we have calculated the NECμM probability in hydrogenlike muonic ^{19}F and ^{16}N. These nuclei possess the lowest-energy electric transitions ($\hbar\omega_N \approx 100\,\mathrm{keV}$) among isotopes with $Z \lesssim 10$. We compare our results with the corresponding ones for hydrogenlike electronic ^{235}U where the isomeric level at 76 eV is reached by an $E3$ transition. This nucleus has been studied most intensively in the literature [40, 103, 105]. For consistency, the ^{235}U system is treated nonrelativistically, although relativistic effects are prominent in deeply bound electron states of highly charged ions. The main parameters of the systems under consideration are summarized in Table 5.1. The atomic binding energy is of the order $\sim 100\,\mathrm{keV}$ in all cases. The atomic extension of the ^{235}U ion is larger by an order of magnitude than the muonic Bohr radii because of the smaller electron mass.

The respective nuclear transition probabilities for laser-driven muonic-^{19}F, muonic-^{16}N and electronic-^{235}U are considered varying with laser intensity as shown in Fig. 5.3. Since, for NECEM/NECμM, the particle should be bound in order to influence the nucleus while oscillating across it, that is why the process before the ionization occurs is important hence, we restrict the curves to terminate at their respective OBI intensities. For this purpose the experimentally obtained parameters have been used for the atoms and the respective nuclei as shown in Table 5.1. Increase of the intensity makes the excitation probability rise in all the three cases. The comparison of these different systems highlights the advantage using the muonic atoms over the electronic-HCI systems since the nucleus excitation probability is order of magnitude higher in contrast with *e.g.*, ^{19}F in case of E1.

It is instructive to comment on various differences with the results presented in [105]. We use the same theoretical approach developed there, however, we apply it to hydrogenlike atoms in the $1s$ state which are moderately affected by an external field such that $u_0 \ll a_0$. In this asymptotic limit we find simple power-law dependences of the excitation probability on the laser intensity (and frequency) [see Eq. (5.15)]. Contrary to that in [105] the collective oscillation of all electrons in higher atomic shells (starting from the 2s orbital) has been considered. The driving laser field was assumed so strong that $u_0 \gtrsim a_0$. In this regime, neglecting field ionization, the excitation probability as a function

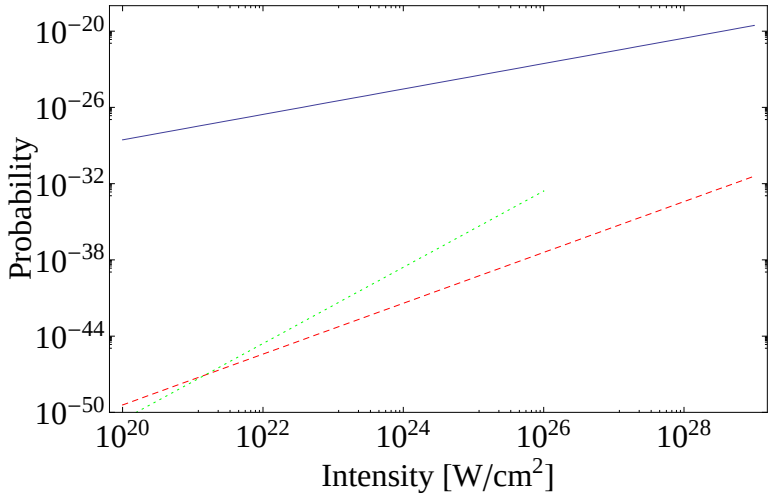

Figure 5.3: Nuclear transition probabilities for laser-driven muonic ^{19}F (blue curve), muonic ^{16}N (red curve), and electronic ^{235}U (green curve), as a function of laser intensity. The laser frequency is $\hbar\omega = 1$eV. The curves stop at the respective OBI intensities.

of intensity first exhibits a power-law increase (with a different exponent, though) and eventually goes through a maximum. The absolute values of the excitation probability are much larger than in our case, but never exceed $P \approx 10^{-11}$ in ^{235}U at 10^{21} W/cm^2 laser intensity and 5eV photon energy.

In Fig. 5.4 we only consider the muonic systems ^{19}F and ^{16}N where $\omega \ll \omega_N$ throughout the plot range. In electronic ^{235}U we would go through a resonance. We take muonic-^{19}F for dipole case and -^{16}N for quadrupole case at laser intensity 10^{26} W/cm^2, because $E_{ip} = 76$ eV only. By increasing the laser frequency the excitation probability enhances but dipole always exceeds the quadrupole result by order of magnitudes as expected.

An alternative way of obtaining higher laser frequencies is to employ (instead of fixed target nuclei) an ion beam which counterpropagates the laser pulse at relativistic speed. In the nuclear rest frame the laser frequency appears Doppler blueshift. In this geometry even a resonant laser-nucleus coupling [114] could be achieved when a bare ^{235}U beam collides at a Lorentz factor $\gamma \approx 30$ with a near-infrared laser beam ($\hbar\omega \approx 1.2\,$eV). The laser Doppler shifted laser frequency $\omega' \approx 2\gamma\omega$ can be tuned into resonance with the nuclear transition frequency. Such an experiment would be taylormade for the future GSI facility where a beam of fully stripped U ions of the required energy will be available, along with the intense PHELIX laser [116].

The nuclear excitation probabilities shown in Figs. 5.3 and 5.4 are very small, but they refer to a single atom. When more than one atom interact with the laser field, the total yield could be increased proportionally. However, intense laser pulses possess a small focal volume only ($V_f \sim 10^{-10}\,$cm^3, to give a typical number), while on the other side it is difficult to produce exotic atoms at very high density. An achievable number density of

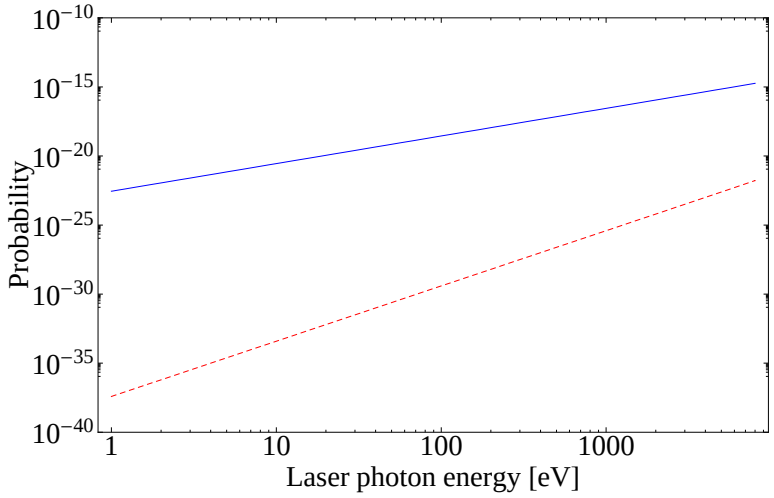

Figure 5.4: Nuclear transition probabilities for laser-driven muonic ^{19}F (blue curve) and ^{16}N (red curve), as a function of laser frequency. The laser intensity is 10^{26} W/cm^2.

trapped muonic atoms is $n \sim 10^{10}$ cm^{-3} which is comparable with the densities available for other exotic species such as positronium (where $n \sim 10^{15}$ cm^{-3} [117]) or antihydrogen (where $n \sim 10^{6}$ cm^{-3} [118]). According to these numbers, only a few muonic atoms are contained in the interaction volume, which prevents a substantial yield enhancement, unfortunately.

Instead of using a fixed target of muonic atoms in a trap, it might therefore be more promising to employ a nonrelativistic beam of muonic atoms. Such beam experiments are in principle feasible and have recently led to the observation of the Ramsauer-Townsend effect in scattering of muonic hydrogen isotopes, for example [119]. Beams of 10^5 muons per second can be produced today [120] which could be converted into the same number of muonic atoms assuming 100% conversion efficiency. The atomic beam could be synchronized with a bunch of laser pulses: at the upcoming XFEL facilities, pulse repetition rates of 40 kHz $\sim 10^5$ s^{-1} are envisaged. In this setup, one muonic atom would interact with one laser pulse at a time. By assuming the highest nuclear excitation probability of about 10^{-14} shown in Fig. 5.4, we obtain a total yield estimate of roughly one excitation event per week. This clearly indicates that an experimental observation of the NECμM process perhaps is not completely impossible, but certainly an extremely challenging task.

Moreover, the NECμM probability is very low, background processes may become competitive or even dominant. First, the maximum intensities considered here are so strong that direct excitation of the nucleus by the laser field cannot be ignored. According to a simple estimate, an upper bound for the probability of this process is $P \lesssim (eE_0 r_N/\hbar\omega_N)^2 \lesssim 10^{-8}$ [1,12]. Besides it is known that the presence of charged particles in ultrastrong laser fields can give rise to nonlinear QED effects like e^+e^- pair creation [65]. They become appreciable when the laser field strength approaches the Schwinger limit $E_S = 1.3 \times 10^{16}$V/cm [121]. Since $E_{\mathrm{OBI}} \lesssim E_S$ for muonic ^{19}F and ^{16}N, the probability for pair creation $P_{e^+e^-} \sim \exp(-\pi E_S/E_0)$ is non-negligible at the borderline of the applicability condition

$E_0 \ll E_{\mathrm{OBI}}$ of our approach.

5.5 Comparison with related processes

Finally, we compare the NECEM/NECμM process with other excitation mechanisms of the nucleus via coupling with atomic states. Most closely related is nuclear excitation in laser-driven recollisions which has been considered recently [16, 18, 113]. Recollisions occur when the applied laser field is strong enough to tunnel-ionize the atom. The liberated electron gains energy during propagation in the field and is driven back to the nucleus when the oscillating field has reversed its direction. Upon recollision, various atomic processes can occur but also nuclear excitation. The recollision-induced excitation probability in electronic ^{239}Pu ($\hbar\omega_N \approx 7.9$ keV) was found to be $P \sim 10^{-16}$ at an optical laser intensity of $\sim 10^{17}\mathrm{W/cm}^2$ [113]. It is larger than the NECEM probabilities found here (see Fig. 5.3). The reason is that the laser field can couple more effectively to a free electron, transferring large amounts of energy to it. In the above example, the electron is accelerated to weakly relativistic energies of about 10 keV. Upon the energetic recollision, the nucleus is excited by electron scattering. The circumstance that free electrons are more efficient for nuclear excitation was also observed in [105] in a hypothetical scenario (see Fig. 7 therein). Similarly, the early papers on NECEM where the electrons were treated as free particles in a first approach [103], obtained large nuclear excitation probabilities (up to $P \sim 0.1$). Such high NECEM probabilities, however, were not confirmed by experiments [41]. More efficient nuclear excitation mechanisms are resonant processes such as (field-free) NEET. They require, however, an atomic inner-shell vacancy which is usually produced by X-ray irradiation first. Contrary to that the NECEM/NECμM process employs atoms in the ground state. In ordinary atoms the NEET probability typically amounts to $P \sim 10^{-7}$ per K-shell vacancy [71, 72, 100]. In muonic atoms the corresponding probability is largely enhanced to $P \sim 0.1$ [73]. It is interesting to note that coherent nuclear (or atomic) excitation in periodic fields can also occur when a fast ion beam is channeling through a crystal. For certain ion velocities a resonance behavior arises here ('Okorokov effect') [122].

Chapter 6

Conclusion and outlook

In this thesis, nuclear effects in muonic atoms in super-intense laser field have been studied. Due to large binding potential it is hard to influence a muonic atom and one needs high frequencies and high intensities. This work is motivated by the upcoming laser facilities where corresponding parameters are envisaged. Keeping these facilities into consideration we restrict ourselves to light isotopes. Essentially, the laser driven muon does not cross the boundary of relativistic regime that is why Schrödinger equation applies. In particular the interest lied in investigating the nuclear properties with the help of radiation spectra. Also, the probability of nuclear excitation by the periodic oscillation of muonic cloud across the nucleus has been taken into account.

In the first project, harmonic response has been investigated by numerically solving the time-dependent Schrödinger equation. The main objective for these calculation is to probe the nuclear signatures for example nuclear mass and size effects, by comparing the HHG spectra for different isotopes of the same atom, *e.g.*, hydrogen versus deuterium. Since lighter nuclei are accelerated more strongly by the laser therefore the maximum photon energy $\hbar\omega_{max}$ obtained is enhanced. This impact of the nuclear mass on the harmonic cutoff position can be understood via the reduced mass which enters the ponderomotive energy of the relative motion. Whereas, the nuclear size and shape influence the plateau height of the spectra. It is due to the fact that the smaller nuclei have steeper potentials that lead to enhanced emission of radiation. For isotopes with $Z > 1$, the laser field couples to muonic atom via an effective charge instead of ordinary muonic charge. This effective charge takes the masses of the nucleus and the muon into account along with the value of Z. The role played by effective charge is clearly visible in the HHG spectra of muonic helium. Apart from the nuclear signatures, the spectra calculated for muonic atoms yield large cutoff energies wich reach up to MeV range that might be used to generate ultra-short X-ray or γ-ray pulses. Our results take us to the realm of the sources to generate attosecond or even zeptosecond pulses.

In the second project, the main emphasis is on nuclear excitation of muonic atoms when placed in super-intense laser fields. The theme is that periodic oscillations of the muonic cloud across the nucleus can excite the nucleus. The closed-form expression for the probability from the ground state to the excited state *i.e.*, $P_{0\to1}$ has been derived by analytical

means, for electric multipoles. This excitation can make a pump-probe scheme conceivable. However, the excitation probabilities found with the muonic atoms are very small, mainly because of the large frequency mismatch between the laser frequency and the excitation frequency (far off resonance).

For an outlook, the coherent ultra-short γ-rays obtained from HHG process can be used for the nuclear photo-excitation. This way, time-resolved nuclear spectroscopy could be feasible. Moreover, other species of exotic atoms could be considered such as pionic atoms. The pion has similar mass as that of the muon. The energy levels in both pionic and muonic atoms are in principal similar. But pionic spectral lines are broadened by the influence of the strong force since the pion can be absorbed by the nucleons of the binding nucleus. This limits the lifetime of light pionic and, in general, hadronic atoms to typical values of $\sim 10^{-15}$ sec. In comparison with muonic atoms or positronium, hadronic atoms cannot be considered as stable in the laser field as their lifetime is on the order of an optical cycle. Pions, being hadrons, are governed by strong forces in contrast with electromagnetic forces as far as muonic atoms are concerned, so by investigating these pionic atoms hadronic interactions can be studied. At first glance, this seems to exclude the possibility of studying their interaction with strong laser fields. To find a remedy to it could be the application of a relativistic atomic beam with Lorentz factor $\gamma \sim 10$ instead of a fixed target [90]. Due to relativistic time dilation, the atomic lifetime is correspondingly enhanced in the lab-frame. By these or similar kind of methods hadronic atoms coupling to intense laser fields could be studied at high laser frequencies ~ 1 keV and/or intensities $\sim 10^{22} - 10^{26}$ W/cm^2.

Our study of nuclear excitation in muonic atoms could be extended by the magnetic multipole transitions. For this purpose suitable isotopes would be used with low nuclear transition energies $\hbar\omega_N$, which in case of heavy isotopes exist. For instance, for M2 transition, ^{229}Th has a transition energy $\hbar\omega_N \approx 7.6$ eV [123]. Heavy muonic atoms, however, ar too tightly bound to be affected by radition from present or near-future laser devices. Highly charged electronic ions appear more promising here. Another example is the E3 transition in ^{235}U, which could be excited directly with the PHELIX laser at GSI when a relativistic ionic beam ($\gamma \sim 30$) is used.

Appendix A

Cut-off law of HHG

We have equation of motion for a free electron in laser field,

$$\frac{d^2x}{dt^2} = \frac{e}{m_e} E_0 \sin(\omega t) \tag{A.1}$$

The three-step model assumes that the electron is released from the atom at time t_0 and at that time it is at rest with respect to the left ion. Then the electron velocity, given by the first integral of Eq. (A.1), will be

$$\frac{dx}{dt} = -\frac{eE_0}{m\omega}(\cos\omega t - \cos\omega t_0)$$

The average K.E. of the electron can be written as

$$\begin{aligned} < K.E. > &= \frac{1}{2}\frac{e^2E_0^2}{m\omega^2} < (\cos\omega t - \cos\omega t_0)^2 > \\ &= \frac{1}{2}\frac{e^2E_0^2}{m\omega^2}\frac{1}{T}\int_{t-0}^{t_0+T}(\cos\omega t - \cos\omega t_0)^2 dt \\ &= \frac{1}{4}\frac{e^2E_0^2}{m\omega^2}(1 + 2\cos^2\omega t_0) \\ &= U_{\mathrm{p}}(1 + 2\cos^2\omega t_0) \end{aligned} \tag{A.2}$$

where T is one laser period.

Determining the system at some particular time t_1 by virtue of [124]

$$0 = \int_{t_0}^{t_1} v(t)dt = \int_{t_0}^{t_1} -\frac{eE_0}{m\omega}(\cos\omega t - \cos\omega t_0)dt$$

$$0 = -\frac{eE_0}{m\omega}(\sin\omega t_1 - \sin\omega t_0) + \frac{eE_0}{m}(t_1 - t_0)\cos\omega t_0$$

Differentiating with respect to t_0 gives,

$$(\cos\omega t - \cos\omega t_0)\frac{\partial t_1}{\partial t_0} = -\omega(t_1 - t_0)\sin\omega t_0.$$

The K.E. at t_1 is

$$E_{\mathtt{kin}}(t_1) = 2U_{\mathtt{p}}(\cos\omega t_1 - \cos\omega t_0)^2$$

Differentiating with respect to ωt_0 leads to

$$\frac{\partial}{\partial\omega t_0}E_{\mathtt{kin}}(t_1) = 0$$

Simultaneously solving the above three equations, we obtain these two equations

$$(\sin\frac{\tau}{2} - \frac{\tau}{2}\cos\frac{\tau}{2})\cos\frac{\sigma}{2} = \frac{\tau}{2}\sin\frac{\tau}{2}\sin\frac{\sigma}{2}$$

and

$$(\sin\frac{\tau}{2} - \frac{\tau}{2}\cos\frac{\tau}{2})\sin\frac{\sigma}{2} = \frac{\tau}{2}\sin\frac{\tau}{2}\cos\frac{\sigma}{2}$$

where $\tau = \omega(t_1 - t_0)$ and $\sigma = \omega(t_1 + t_0)$. Dividing both the equations provides

$$\sigma_k = 2k\pi \pm \frac{\pi}{2}$$

having k is some integer. Hence the K.E. becomes

$$E_{\mathtt{kin}}(t_1) = 4U_{\mathtt{p}}\sin^2\frac{\tau_k}{2}$$

From recurrence times τ_k the maximum energy is obtained at $k = 1$ which makes the relation

$$E_{\mathtt{kin}}(t_1) = 3.173U_{\mathtt{p}}.$$

which implies the cutoff formula (2.13).

Appendix B

Separation without dipole approximation

In this appendix we show that the two-particle Schrödinger equation (B.1) does not separate without application of the dipole approximation to the laser field. To this end we include the next-order term beyond the dipole approximation. Then the two-particle Schrödinger equation becomes [125]

$$i\hbar\frac{\partial}{\partial t}\psi\left(\mathbf{r}_1,\mathbf{r}_2,t\right)=\left[\frac{\mathbf{p}_1^2}{2m_1}+\frac{\mathbf{p}_2^2}{2m_2}+\left\{\mathbf{r}_1+\mathbf{r}_2-\frac{i}{c}(\hat{\mathbf{k}}.\mathbf{r}_1)\bigtriangledown_1+\frac{iZ}{c}(\hat{\mathbf{k}}.\mathbf{r}_2)\bigtriangledown_2\right\}.\mathbf{E}(t)\right]\psi\left(\mathbf{r}_1,\mathbf{r}_2,t\right) \tag{B.1}$$

where $\hat{\mathbf{k}}$ denotes a unit vector in laser propagation direction and $\mathbf{p}_1=-i\hbar\bigtriangledown_{\mathbf{1}}$ and $\mathbf{p}_2=-i\hbar\bigtriangledown_{\mathbf{2}}$. If $\mathbf{r}_1$ and $\mathbf{r}_2$ are the corresponding vectors for the two bodies of mass m_1 and m_2, respectively, then the resultant vector for the center of mass and relative coordinates can be written as

$$\mathbf{R}=\frac{m_1\mathbf{r}_1+m_2\mathbf{r}_2}{m_1+m_2} \tag{B.2}$$

$$\mathbf{r}=\mathbf{r}_1-\mathbf{r}_2 \tag{B.3}$$

where

$$\mathbf{r}_1=\mathbf{R}+\left(\frac{m_2}{m_1+m_2}\right)\mathbf{r} \tag{B.4}$$

and

$$\mathbf{r}_2=\mathbf{R}-\left(\frac{m_1}{m_1+m_2}\right)\mathbf{r}. \tag{B.5}$$

Also,

$$\bigtriangledown_1=\bigtriangledown_r+\left(\frac{m_1}{m_1+m_2}\right)\bigtriangledown_R \tag{B.6}$$

$$\bigtriangledown_2=-\bigtriangledown_r+\left(\frac{m_2}{m_1+m_2}\right)\bigtriangledown_R \tag{B.7}$$

Simultaneous dealing of the above equation lead us to

$$\nabla_1^2 = \nabla_r^2 + \left(\frac{m_1}{m_1+m_2}\right)^2 \nabla_R^2 + 2\frac{m_1}{m_1+m_2}\,\nabla_r \cdot \nabla_R \tag{B.8}$$

$$\nabla_2^2 = \nabla_r^2 + \left(\frac{m_2}{m_1+m_2}\right)^2 \nabla_R^2 - 2\frac{m_2}{m_1+m_2}\,\nabla_r \cdot \nabla_R \tag{B.9}$$

and Eq. (B.1) becomes

$$\begin{aligned} i\hbar\frac{\partial}{\partial t}\psi(\mathbf{r},\mathbf{R},t) = \Bigg[& -\frac{\hbar^2}{2m_1}\left\{\nabla_r^2 + \left(\frac{m_1}{m_1+m_2}\right)^2 \nabla_R^2 + 2\left(\frac{m_1}{m_1+m_2}\right)\nabla_r \cdot \nabla_R\right\} \\ & -\frac{\hbar^2}{2m_2}\left\{\nabla_r^2 + \left(\frac{m_2}{m_1+m_2}\right)^2 \nabla_R^2 - 2\left(\frac{m_2}{m_1+m_2}\right)\nabla_r \cdot \nabla_R\right\} \\ & + \Bigg(\mathbf{R} + \left(\frac{m_2}{m_1+m_2}\right)\mathbf{r} + \mathbf{R} - \left(\frac{m_1}{m_1+m_2}\right)\mathbf{r} \\ & - \frac{i}{c}\left\{\mathbf{k}.\left(\mathbf{R} + \left(\frac{m_2}{m_1+m_2}\right)\mathbf{r}\right)\nabla_r + \left(\frac{m_1}{m_1+m_2}\right)\nabla_R\right\} \\ & + \frac{iZ}{c}\Bigg\{\mathbf{k}.\left(\mathbf{R} - \left(\frac{m_1}{m_1+m_2}\right)\mathbf{r}\right) \\ & \times\left(-\nabla_r + \left(\frac{m_2}{m_1+m_2}\right)\nabla_R\right)\Bigg\}\Bigg).\mathbf{E}(t)\Bigg]\psi(\mathbf{r},\mathbf{R},t) \end{aligned} \tag{B.10}$$

which simplifies to

$$\begin{aligned} i\hbar\frac{\partial}{\partial t}\psi(\mathbf{r},\mathbf{R},t) \;=\; & \Bigg[-\frac{\hbar^2}{2m_{red}}\nabla_r^2 - \frac{\hbar^2}{2(m_1+m_2)}\nabla_R^2 \\ & + (2\mathbf{R} + \left(\frac{m_2-m_1}{m_1+m_2}\right)\mathbf{r}).\mathbf{E} + \text{Crossed Terms}\Bigg]\psi(\mathbf{r},\mathbf{R},t) \end{aligned} \tag{B.11}$$

The appearance of cross terms containing both relative and center-of-mass coordinates prevents the equation from being separable.

Appendix C

Crank Nicholson Scheme

The Crank Nicholson scheme is a finite difference method used numerically. It is second-order in time and is numerically stable [126].

A finite difference is like a differential quotient, except that it uses finite quantities instead of infinitesimal ones. The derivative of a function f at a point x is defined by the limit

$$\frac{df}{dx} = \lim_{h \to 0} \frac{f(x+h) - f(x)}{h}$$

If h has a fixed (non-zero) value, instead of approaching zero, this quotient is called a finite difference.

$$\frac{\triangle f}{\triangle x} = \frac{f(x+h) - f(x)}{h}$$

This method involves taking the derivative half way between the beginning and the end of the space. It is hence an average between a fully implicit and fully explicit model of partial differential equations.

Parabolic partial differential equation

The time-dependent one-dimensional diffusion equation can be written as

$$\frac{\partial u}{\partial t} = d\frac{\partial^2 u}{\partial x^2} \tag{C.1}$$

where u is the temperature distribution on a long thin rod of constant cross-section and uniform heat conducting material and d is the ratio between the thermal conductivity and heat capacity. The forward difference approximation for the time derivative in the one dimensional heat equation Eq. (C.1) can be written as

$$\frac{u_i^{n+1} - u_i^n}{\triangle t} = d\frac{u_{i-1}^n - 2u_i^n + u_{i+1}^n}{\triangle x^2} \tag{C.2}$$

where $i = 0, 1, 2, \cdots, N$ labels positions and $n = 0, 1, 2, \cdots$ labels instants of time. It gives a formula to compute the unknown temperature distribution on the rod at various

positions at various times. Namely, from Eq. (C.2)

$$u_i^{n+1} = u_i^n + r(u_{i-1}^n - 2u_i^n + u_{i+1}^n) \tag{C.3}$$

with $r = d\frac{\triangle t}{\triangle x^2}$. This method is called Forward time and central space (FTCS).

Since this formula has only one unknown for any i and n it is called an explicit scheme.

If the things are replaced with the backward difference then

$$\frac{u_i^{n+1} - u_i^n}{\triangle t} = d\frac{u_{i-1}^{n+1} - 2u_i^{n+1} + u_{i+1}^{n+1}}{\triangle x^2} \tag{C.4}$$

where $i = 1, 2, \cdots, N-1$ and $n = 0, 1, 2, \cdots$.

From Eq. (C.4)

$$u_i^{n+1} - u_i^n = r(u_{i-1}^{n+1} - 2u_i^{n+1} + u_{i+1}^{n+1}). \tag{C.5}$$

Since there are three unknown terms, the scheme so obtained is an implicit scheme.

The main drawback of having more than one unknown coefficient in any equation, unlike FTCS method, is value of the dependent variable at any typical node say (i, n) cannot be obtained from the single finite difference equation of the node (i, n) but one has to generate a system of equations for each time level separately by varying i. Then for each time level there will be system of equations equivalent to the number of unknowns in that time level (say $N-1$ in the present case). This linear system of algebraic equations in $N-1$ unknowns has to be solved to obtain the solution for each time level. This process has to be repeated until the desired time level is reached.

Explicit and implicit schemes are two different methods to solve the one dimensional heat equation Eq.(C.1). Crank Nicholson scheme is then obtained by taking average of these two schemes *i.e.*,

$$\frac{u_i^{n+1} - u_i^n}{\triangle t} = \frac{d}{2}\left[\frac{u_{i-1}^{n+1} - 2u_i^{n+1} + u_{i+1}^{n+1}}{\triangle x^2} + \frac{u_{i-1}^n - 2u_i^n + u_{i+1}^n}{\triangle x^2}\right] \tag{C.6}$$

for $i = 1, 2, \cdots, N-1$ and $n = 0, 1, 2, \cdots$. It can be proved that Crank Nicholson scheme is second order in space and time.

Crank Nicholson scheme for TDSE

The time-dependent Schrödinger equation in one dimension

$$\frac{\partial\psi(x,t)}{\partial t} = \frac{i\hbar}{2m}\frac{\partial^2\psi(x,t)}{\partial x^2} - i\frac{V(x)}{\hbar}\psi(x,t) \tag{C.7}$$

is a parabolic partial differential equation. The solution is considered on an interval from $a \leq x \leq b$ and $t > 0$. The solution is determined from boundary conditions:

$$\psi(a,t) = \psi(b,t) = 0$$

and

$$\psi(x,0) = f(x)$$

One method for numerical solution solves for the values of the wavefunction on a regular grid of dimension

$$h = \frac{b-a}{N_x}$$

in x and τ in t:

$$\psi_j^l = \psi(a+jh, l\tau). \tag{C.8}$$

The derivatives are replaced by simple finite differences. The right side of the equation at the grid point (l, j) is then

$$\frac{i\hbar}{2mh^2}(\psi_j^{l+1} + \psi_{j-1}^l - 2\psi_j^l) - i\frac{V(a+jh)}{\hbar}\psi_j^l = \sum_{m=0}^{N} iH_{j,m}\psi_m^l \tag{C.9}$$

where H is a real symmetric tridiagonal matrix (provided $V(x)$ is real). The left side of the equation can be replaced either by a forward difference

$$\frac{\psi_j^{l+1} - \psi_j^l}{\tau},$$

which, when combined with the right hand side, gives the explicit algorithm

$$\psi^{l+1} = (1 + iH\tau)\psi^l, \tag{C.10}$$

or by a backward difference

$$\frac{\psi_j^l - \psi_j^{l-1}}{\tau},$$

leading to

$$\psi^l = \psi^{l-1} + iH\tau\psi^l, \tag{C.11}$$

or (with the replacement $l \to l+1$), the implicit algorithm

$$(1 - iH\tau)\psi^{l+1} = \psi^l. \tag{C.12}$$

Averaging the Eqs. (C.10) and (C.12):

$$\left(1 - iH\frac{\tau}{2}\right)\psi^{l+1} = \left(1 + iH\frac{\tau}{2}\right)\psi^l. \tag{C.13}$$

This method is a second order algorithm in t, *i.e.* the discretization error decreases as τ^2. The finite difference representation of the second derivative d^2/dx^2 is also good to second order in h^2. The Crank-Nicholson Algorithm gives a unitary evolution in time. That is especially useful for quantum mechanics where unitarity assures that the normalization of the wavefunction is unchanged over time.

Imaginary time propagation

The Crank-Nicholson method is a stable routine for numerically solving time-dependent Schrödinger-like equations. Integrating the Schrödinger equation

$$i\frac{\partial\psi}{\partial t} = H\psi$$

leads to the time evolution of the wavefunction after a time interval $\triangle t$

$$\psi(r, t + \triangle t) = \exp(-i\triangle t H)\psi(r, t) + O(\triangle t^2). \tag{C.14}$$

It assumes that the hamiltonian H does not vary over this time interval.

A reliable method to obtain the ground state of the system employs propagation in imaginary time. Consider the wavefunction as a superposition of eigenstates $\theta_m(r)$ with time-dependent amplitudes $a_m(t)$ and eigen energies E_m. Substituting $\triangle t \rightarrow -i\triangle t$, the wavefunction in the above equation (C.14) decays exponentially

$$\psi(r, t + \triangle t) = \sum_m a_m(t)\theta_m(r)\exp(-E_m\triangle t) \tag{C.15}$$

The ground state of the system decays with the slowest rate. By suitable renormalisation of the wavefunction during the imaginary time propagation, the wavefunction moves towards the ground state of the system.

Time convergence for our calculations

The HHG spectra are calculated in this thesis by solving TDSE with the help of Crank Nicholson scheme. To emphasize that our calculations are convergent as far as time steps are concerned we draw it graphically in Fig. C.1. The plot represents the cutoff position against the number of time steps. Our calculations employ 2.5×10^6 time steps which guarantees clear that it converges at this number.

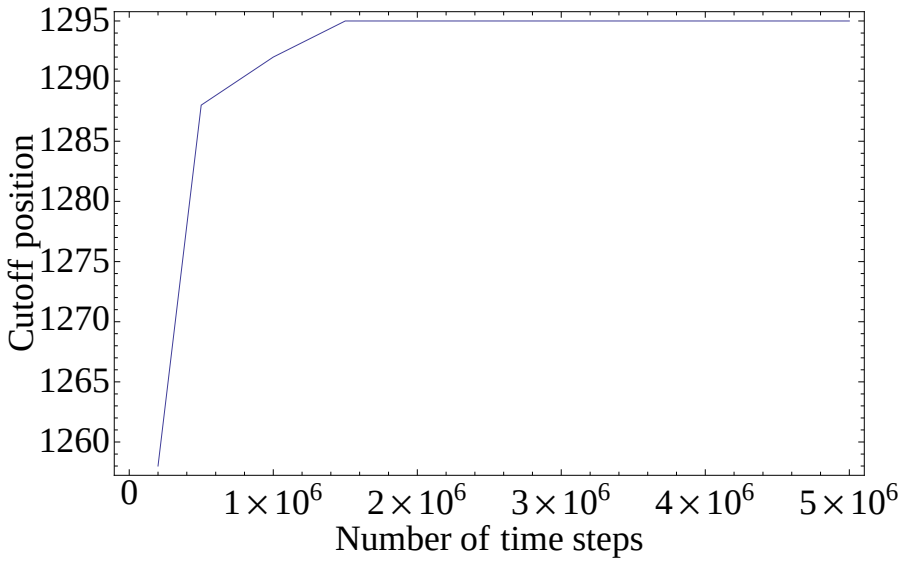

Figure C.1: The time convergence plot for muonic hydrogen atom in nuclear size effect. The plot shows the harmonic order at the cutoff position as a function of time steps considered for the numerical evaluation for the dipole acceleration.

Appendix D

Dipole, quadrupole and octupole transitions

Dipole

For dipole transitions the difference on angular momentum is $\lambda = 1$. In our case $\mu = 0$ due to cylinderical symmetry, so that the relevant spherical harmonic is

$$Y_1^0(\Omega) = \frac{1}{2}\sqrt{\frac{3}{\pi}}\cos\theta \tag{D.1}$$

and the Eq. (5.7) for transition for dipole is

$$F_1^0(t) = \int_0^\infty \int_0^{2\pi} \int_{-1}^{1} \frac{r^2}{r^2} dr d\phi d\cos\theta e^{-(r^2 - 2r\cos\theta u(t) + u(t)^2)} \frac{1}{2}\sqrt{\frac{3}{\pi}}\cos\theta \tag{D.2}$$

regarding $\xi = \cos\theta$

$$F_1^0(t) = \frac{1}{2}\sqrt{\frac{3}{\pi}} \int_0^\infty \int_0^{2\pi} \int_{-1}^{1} \frac{r^2}{r^2} \xi dr d\phi d\xi e^{-(r^2 - 2r\xi u(t) + u(t)^2)} \tag{D.3}$$

After the elementary integration the relation obtained is:

$$F_1(t) = \frac{\sqrt{3}}{2\pi u^2}\left[\sqrt{\pi}\mathrm{Erf}(x) - 2xe^{-x^2}\right] \tag{D.4}$$

Quadrupole

For quadrupole $\lambda = 2$

$$Y_2^0(\Omega) = \frac{1}{4}\sqrt{\frac{5}{\pi}}(3\cos^2\theta - 1) \tag{D.5}$$

and final relation for quadrupole transition obtained is:

$$F_2(t) = \frac{\sqrt{5}}{2\pi u^3}\left[\sqrt{\pi}\mathrm{Erf}(x) - \left(2x + \frac{4}{3}x^3\right)e^{-x^2}\right] \tag{D.6}$$

Octupole

Similarly for octupole $\lambda = 3$

$$Y_3^0(\Omega) = \frac{1}{4}\sqrt{\frac{7}{\pi}}(5\cos^3\theta - 3\cos\theta) \tag{D.7}$$

and final relation for octupole transition obtained is:

$$F_3(t) = \frac{\sqrt{7}}{2\pi u^4}\left[\sqrt{\pi}\mathrm{Erf}(x) - \left(2x + \frac{4}{3}x^3 + \frac{8}{15}x^5\right)e^{-x^2}\right]. \tag{D.8}$$

Bibliography

[1] S. Matinyan, Phys. Rep. **298**, 199 (1998).

[2] Y. I. Salamin, S. X. Hu, K. Z. Hatsagortsyan and C. H. Keitel, Phys. Rep. **427**, 41 (2006).

[3] H. Schwoerer, J. Magill, and B. Beleites (Eds.), *Lasers and Nuclei* (Springer, Heidelberg, 2006).

[4] R. Neugart, Eur. Phys. J. **A 15**, 35 (2002).

[5] K. W. D. Ledingham *et al.*, Phys. Rev. Lett. **84**, 899 (2000); T. E. Cowan *et al.*, *ibid.* **84**, 903 (2000).

[6] T. Ditmire *et al.*, Nature (London) **398**, 489 (1999).

[7] D. Umstadter, J. Phys. **D 36**, R151 (2003).

[8] K. W. D. Ledingham, P. McKenna, and R. P. Singhal, Science **300**, 1107 (2003).

[9] V. Yanovsky *et al.*, Opt. Express **16**, 2109 (2008).

[10] http://www.eli-laser.eu/

[11] Gerstner, Extreme Light, Nature **446**, 16 (2007).

[12] T. J. Bürvenich, J. Evers, and C. H. Keitel, Phys. Rev. Lett. **96**, 142501 (2006).

[13] A. Pálffy, J. Evers, and C. H. Keitel, Phys. Rev. **C 77**, 044602 (2008).

[14] K. Z. Hatsagortsyan *et al.*, J. Opt. Soc. Am. **B 25**, B92 (2008); M. Klaiber, K. Z. Hatsagortsyan, and C. H. Keitel, arXiv: 0707.2900 [atom-ph].

[15] M. Klaiber, K. Z. Hatsagortsyan, and C. H. Keitel, Phys. Rev. **A 75**, 063413 (2007).

[16] N. Milosevic, P. B. Corkum, and T. Brabec, Phys. Rev. Lett. **92**, 013002 (2004).

[17] M. Casu and C. H. Keitel, Europhys Lett. **58**, 496 (2002).

[18] G. R. Mocken and C. H. Keitel, J. Phys. **B 37**, L275 (2004).

[19] B. Henrich, K. Z. Hatsagortsyan and C. H. Keitel, Phys. Rev. Lett. **93**, 013601 (2004).

[20] C. Müller, K. Z. Hatsagortsyan and C. H. Keitel, Physics Letters **B 659**, 209 (2008).

[21] Y. S. Kim, *Mesic Atoms and Nuclear Structure* (North-Holland, Amsterdam, 1971); J. M. Eisenberg and W. Greiner, *Nuclear Theory, Vol. 2: Excitation Mechanisms of the Nucleus* (North-Holland, Amsterdam, 1976).

[22] C. S. Wu and L. Wilets, Annu. Rev. Nucl. Sci. **19**, 527 (1969); M. I. Eides, H. Grotch, and V. A. Shelyuto, Phys. Rep. **342**, 63 (2001).

[23] E. Borie and G. A. Rinker, Rev. Mod. Phys. **54**, 67 (1982).

[24] V. L. Fitch and J. Rainwater, Phys. Rev. **92**, 789 (1953).

[25] B. M. Forster *et al.*, Hyperfine Interact. **65**, 1007 (1991); D. H. Wright *et al.*, Nucl. Instrum. Meth. Phys. Res. **A 320**, 249 (1992).

[26] T. Nilsson, J. Äystö, K. Langanke, K. Riisager, G. Martinez-Pinedo, and E. Kolbe, Nucl. Phys. **A 746**, 513 (2004).

[27] W. H. Breunlich and P. Kammel, Annu. Rev. Nucl. Part. Sci. **39**, 311 (1989).

[28] W. Becker *et al.*, Adv. At. Mol. Opt. Phys. **48**, 35 (2002); D. B. Milošević and F. Ehlotzky, *ibid.* **49**, 373 (2003).

[29] A. Shahbaz, C. Müller, A. Staudt, T. J. Bürvenich, and C. H. Keitel, Phys. Rev. Lett. **98**, 263901 (2007).

[30] S. Chelkowski, A. D. Bandrauk, and P. B. Corkum, Phys. Rev. Lett. **93**, 083602 (2004).

[31] M. Kalinski, Las. Phys. **15**, 1367 (2005); R. Schützhold, G. Schaller, and D. Habs, Phys. Rev. Lett. **97**, 121302 (2006).

[32] M. Morita, Prog. Theor. Phys. **49**, 1574 (1973).

[33] E. V. Tkalya, Nucl. Phys. **A 539**, 209 (1992).

[34] M. R. Harston and J. F. Chemin, Phys. Rev. **C 59**, 2462 (1999).

[35] V. Gol'danskii and V. A. Namiot, Phys. Lett. **B 62**, 393 (1976); J. C. Kimball, D. Bittle, and N. Cue, Phys. Lett. **A 152**, 367 (1991); A. Pálffy, Z. Harman, C. Kozhuharov, C. Brandau, C. H. Keitel, W. Scheid and T. Stöhlker, Phys. Lett. **B 661**, 330 (2008).

[36] W. B. Kaufmann and H. Pilkuhn, Z. Physik **A 280**, 283 (1977); A. V. Glushkov and L. N. Ivanov, Phys. Lett. **A 170**, 33 (1992). *Recent Adv. Theor. Phys. Chem. Syst.*, Prog. Theor. Chem. Phys., Vol. **15**, edited by J. P. Julien *et al.*, (Springer, Amsterdam, 2006), p. 301.

[37] A. Pálffy, J. Evers, and C. H. Keitel, Phys. Rev. Lett. **99**, 172502 (2007).

[38] G. C. Baldwin and J. C. Solem, Rev. Mod. Phys. **69**, 1085 (1997).

[39] Berger *et al.*, Phys. Rev. **A 43**, 455 (1991).

[40] F. X. Hartmann, D. W. Noid, and Y. Y. Sharon, Phys. Rev. **A 44**, 3210 (1991).

[41] J. A. Bounds and P. Dyer, Phys. Rev. **C 46**, 852 (1992).

[42] Claverie *et al.*, Phys. Rev. **C 70**, 044303 (2004).

[43] http://www.engin.umich.edu/research/cuos/

[44] http://www.clf.rl.ac.uk/Facilities/vulcan/laser.htm

[45] http://www.gsi.de/forschung/phelix/

[46] For current information on the FLASH facility see http://www-hasylab.desy.de/facility/fel

[47] G. D. Tsakiris *et al.*, New J. Phys. **8**, 19 (2006); A. Pukhov, Nature Physics **2**, 439 (2006).

[48] F. Fabre, G. Petite, P. Agostini and M. Clement, J. Phys. **B 15**,1353 (1982).

[49] L. V. Keldysh, Sov. Phys. JETP **20**, 1307 (1965).

[50] D. M. Volkov, Z. Phys. **94**, 250 (1935).

[51] P. B. Corkum, Phys. Rev. Lett. **71**, 1994 (1993).

[52] K. J. Schafer, B. Yang, L. DiMauro and K. C. Kulander, Phys. Rev. Lett. **70**, 1599 (1993).

[53] M. Lewenstein, P. Balcou, M. Y. Ivanov, LHuiller and P. B. Corkum, Phys. Rev. **A 49**, 2117 (1994).

[54] I. A. McPherson *et al.*, J. Opt. Soc. Am. **B 4**, 595 (1987).

[55] C. L. Gordon III, Phys. Rev. Lett. **70**, 766 (1993).

[56] T. Brabec and F. Krausz., Rev. Mod. Phys. **72**, 545 (2000).

[57] I. P. Christov, M. M. Murnane and H. C. Kapteyn, Phys. Rev. Lett. **78**, 1251 (1997).

[58] M. Bauer *et al.*, Phys. Rev. Lett. **87**, 025501 (2001).

[59] M. Protopapas *et al.*, Rep. Prog. Phys. **60**, 389 (1997).

[60] C. J. Joachain *et al.*, Adv. At. Mol. Opt. Phys. **42**, 225 (2000).

[61] C. H. Keitel, Contemp. Phys. **42**, 353 (2001).

[62] A. Maquet and R. Grobe, J. Mod. Opt. **49**, 2001 (2002).

[63] J. Seres *et al.*, Nature **433**, 596 (2005).

[64] C. Bula *et al.*, Phys. Rev. Lett. **76**, 3116 (1996); L. S. Brown and W. B. Kibble, Phys. Rev. **133**, A705 (1964).

[65] D. Burke *et al.*, Phys. Rev. Lett. **79**, 1626 (1997).

[66] C. Gahn *et al.*, Appl. Phys. Lett. **77**, 2662 (2000).

[67] C. Gahn *et al.*, Phys. Plasmas **9**, 987 (2002).

[68] E. Fermi and E. Teller, Phys. Rev. **72**, 399 (1947).

[69] Y. N. Kim, Mesic Atoms and Nuclear Structure (North Holland, Amsterdam, 1971).

[70] M. C. Fujiwara *et al.*, Phys. Rev. Lett. **85**, 1642 (2000); F. Mulhauser *et al.*, Phys. Rev. **A 73**, 034501 (2006).

[71] K. Otozai, R. Arakawa, and M. Morita, Prog. Theor. Phys. **50**, 1771 (1973); Y. Izawa and C. Yamanaka, Phys. Lett. **B 88**, 59 (1979); H. Fujioka *et al.*, Z. Phys. **A 315** - Atoms and Nuclei, 121 (1984); I. Ahmad *et al.*, Phys. Rev. **C 61**, 051304 (2000); K. Aoki *et al.*, Phys. Rev. **C 64**, 044609 (2001).

[72] Kishimoto *et al.*, Phys. Rev. Lett. **85**, 1831 (2000).

[73] M. Ya. Balats *et al.*, Zh. Eksp. Teor. Fiz. **38**, 1715 (1960) [Sov. Phys. JETP **11**, 1239 (1960)].

[74] D. F. Zaretski and V. M. Novikov, Nucl. Phys. **28**, 177 (1961).

[75] F. F. Karpeshin and V. O. Nesterenko, J. Phys. **G 17**, 705 (1991).

[76] L. Wilets, Kgl. Danske. Vindenskab. Selskab, Mat.-Fys. **29**, No. 3 (1954); B. A. Jacobsohn, Phys. Rev. **96**, 1637 (1954).

[77] Dz. Ganzorig, *et al.*, Nucl. Phys. **A 380**, 278 (1980).

[78] W. Greiner, Relativistic Quantum Mechanics (Berlin: Springer, 1990).

[79] G. Carboni *et al.*, Nucl. Phys. **A 278**, 381 (1977); R. T. Robiscoe and M. Simonious, Phys. Lett. **A 85**, 30 (1981).

[80] N. R. Newbury *et al.*, Phys. Rev. Lett. **67**, 3219 (1991); P. A. Souder, Z. Phys. **C 56**, 146 (1992).

[81] L. B. Madsen and P. Lambropoulos, Phys. Rev. **A 59**, 4574 (1999).

[82] J. H. Eberly *et al.*, in: *Atoms in Intense Laser Fields*, edited by M. Gavrila (Academic Press, San Diego, 1992).

[83] U. Schwengelbeck and F. H. M. Faisal, Phys. Rev. **A 50**, 632 (1994).

[84] I. P. Christov *et al.*, Phys. Rev. Lett. **77**, 1743 (1996).

[85] A. Gordon, R. Santra, and F. X. Kärtner, Phys. Rev. **A 72**, 063411 (2005).

[86] B. Povh, K. Rith, C. Scholz, and F. Zetsche, *Particles and Nuclei* (Springer, Berlin, 2006).

[87] See *e.g.*, C. Figueira de Morisson Faria *et al.*, Phys. Rev. **A 65**, 023404 (2002); R. Taïeb *et al.*, Phys. Rev. **A 68**, 033403 (2003); H. Niikura, D. M. Villeneuve, and P. B. Corkum, Phys. Rev. Lett. **94**, 083003 (2005).

[88] See *e.g.*, S. Palaniyappan *et al.*, Phys. Rev. **A 74**, 033403 (2006).

[89] C. Müller, A. B. Voitkiv, and N. Grün, Phys. Rev. Lett. **91**, 223601 (2003); C. C. Chirilă *et al.*, *ibid.* **93**, 243603 (2004).

[90] U. I. Uggerhøj, Phys. Rev. **A 73**, 052705 (2006).

[91] P. J. Mohr and B. N. Taylor, Rev. Mod. Phys. **77**, 1 (2005).

[92] S. X. Hu *et al.*, J. Phys. **B 35**, 627 (2002).

[93] J. W. Rohlf, *Modern Physics from α to Z^0* (John Wiley & Sons, Inc. New York, 1994).

[94] I. Angeli, At. Data Nucl. Data Tables **87**, 185 (2004).

[95] R. C. Nayak and L. Satpathy, At. Data Nucl. Data Tables **73**, 213 (1999).

[96] N. L. Manakov, private communication; see also M. V. Frolov *et al.*, Phys. Rev. **A 75**, 063408 (2007).

[97] K. D. Schultz *et al.*, J. Mod. Opt. **54**, 1075 (2007).

[98] C. Brandau *et al.*, Phys. Rev. Lett. **100**, 073201 (2008).

[99] C. Müller *et al.*, Progress Report No. **3** of the PHELIX theory group, Ed. P. Mulser, GSI Report 2008-05, April 2008, 26 (GSI, Darmstadt, Germany, 2008).

[100] K. Otozai. R. Arakawa, and T. Saito, Nucl. Phys. **A 297**, 97 (1978);

[101] T. Saito, A. Shinohara, and K. Otozai, Phys. Lett. **B 92**, 293 (1980).

[102] M. Jung *et al.*, Phys. Rev. Lett. **86**, 983 (2001).

[103] J. C. Solem, and L. C. Biedenharn, J. Quant. Spectrosc. Radiat. Transfer, **40**, 707 (1988).

[104] L. C. Biedenharn, G. A. Rinker, and J. C. Solem. Journal of the Optical Society of America **B**: Optical Physics, 221 (1989).

[105] J. F. Berger, D. M. Gogny, and M. S. Weiss, Phys. Rev. **A 43**, 455 (1991).

[106] for a similar process see P. Kálmán and T. Keszthelyi, Phys. Rev. **A 47**, 1320 (1993).

[107] S. Typel, and C. Leclercq-Willain, Phys. Rev. **A 53**, 2547 (1996).

[108] P. Christillin, A. Dellafiore and M. Rosa-Clot, Phys. Rev. Lett. **31**, 1012 (1973); B. Goulard, and H. Primakoff, Phys. Rev. **C 10**, 2034 (1974); W. B. Kaufmann, and H. Pilkuhn, Z. Physik **A 280**, 283 (1977).

[109] W. B. Rolnick, Phys. Rev. **132**, 1110 (1963).

[110] R. Baader, *et al.*, Phys. Lett. **B 27**, 428 (1968).

[111] The analogous, purely atomic effect of inner-shell excitation by coherent motion of outer-shell electrons in a strong driving laser field has been proposed in K. Boyer and C. K. Rhodes, Phys. Rev. Lett. **54**, 1490 (1985).

[112] S. Vivirito, K. T. Taylor, and J. S. Parker, J. Phys. **B 32**, 3015 (1999); G. van de Sand and J. M. Rost, Phys. Rev. **A 62**, 053403 (2000); A. Ljubičić, D. Kekez and B. A. Logan, Phys. Lett. **B 272**, 1 (1991).

[113] A. S. Kornev and B. A. Zon, Laser Phys. Lett. **4**, 588 (2007).

[114] T. J. Bürvenich, J. Evers, and C. H. Keitel, Phys. Rev. **C 74**, 044601 (2006).

[115] F. Ajzenberg-Selove, Nucl. Phys. **A 392**, 1 (1983); D. R. Tilley, H. R. Weller, and C. M. Cheves, Nucl. Phys. **A 565**, 1 (1993).

[116] D. H. H. Hoffmann *et al.*, Laser Part. Beams **23**, 47 (2005).

[117] D. B. Cassidy *et al.*, Phys. Rev. Lett. **95**, 195006 (2005); D. B. Cassidy and A. P. Mills, Jr., Nature **449**, 195 (2007).

[118] M. Amoretti *et al.*, Nature **419**, 456 (2002).

[119] F. Mulhauser *et al.*, Phys. Rev. **A 73**, 034501 (2006).

[120] T. J. Stocki *et al.*, Nucl. Phys. **A 697**, 55 (2002).

[121] A. Ringwald, Phys. Lett. **B 510**, p. 107 (2001).

[122] V. V. Okorokov, Yad. Fiz. **2**, 1009 (1965) [Sov. J. Nucl. Phys. **2**, 719 (1966)].

[123] B. R. Beck *et al.*, Phys. Rev. Lett. **98**, 142501 (2007).

[124] W. Becker, S. Long, and J. K. McIver, Phys. Rev. **A 50**, 1540 (1994).

[125] C. C. Chirilă *et al.*, Phys. Rev. A **66**, 063411 (2002).

[126] J. R. Hiller, I. D. Johnston und D. F. Styer, Quantum Mechanic Simulations, Wiley, New York (1995).

Acknowledgment

I humbly thank Almighty Allah, the most Merciful and the most Beneficent, who gave me health, thoughts and co-operative people to enable me achieve this goal. I am deeply indebted to my adviser, Professor Christoph H. Keitel, for his guidance and support. The deepest regards, no doubt, go to none other than Dr. Carsten Müller and Dr. Thomas Bürvenich for their continuous guidance throughout this work. They mentored and supported me with passion. Without their help, this work would not be possible. Their advice and patience are highly appreciated.

I extend my acknowledgment to Dr. Andreas Staudt who provided and guided me with his code.

Special regards go to Peter Brunner, who is an ever-ready person and do not let our time go wasted as far as computational facilities are concerned. Alongwith him the secretaries first Martina Weizmann and after her Vera Beyer were pretty helpful when I needed them. Also, our librarian Gernot Vogt was very nice and friendly to me.

I am grateful to my office-mates specially Erik Lötstedt, Henrik Hetzheim, Mrityunjay Kundu, Elmar van der Zwan, Benedikt Wundt, Qurrat-ul-Ain Gulfam, Carlus Deneke, Bastian Jungnitsch, Luling Jin and many more for establishing such a nice atmosphere of our room having some chit chats on different topics. Other colleagues were also very friendly and nice specially I had very nice equations with Dr. Zoltán Harman, Martin Haas, Matthias Ruf, Octavian Postavaru, Hossein Ebadi, Dr. Bennaceur Najjari .

The faculty members PD Dr. Dieter Bauer, PD Dr. Jörg Evers, Dr. Karen Z. Hatsagortsyan and PD Dr. Ulrich D. Jentschura were also very helpful and friendly.

Also, I would like to acknowledge my friends outside the institute, they have been extremely very helpful as far as my social life is concerned.

Special thanks to Higher Education Commission (HEC), Pakistan for providing me the financial assistance for my Ph.D., DAAD for taking care in Germany, Max-Planck-Institute for Nuclear Physics for providing me workspace and GC University, Lahore for granting me leave for my Ph.D.

Last but not the least, I would like to say thanks to my family: my mother, brother and sisters and the two little nieces whom I have never seen.